Report No. FRA-ORDD 75-7

UILU-ENG-74-2025

CONCRETE FOR TUNNEL LINERS:
BEHAVIOR OF STEEL FIBER REINFORCED CONCRETE UNDER COMBINED LOADS

Kenneth S. Herring
Clyde E. Kesler

Department of Civil Engineering
University of Illinois
Urbana, Illinois

AUGUST 1974

FINAL REPORT

Document is available to the public through the
National Technical Information Service
Springfield, Virginia 22151

Prepared for

Department of Transportation
FEDERAL RAILROAD ADMINISTRATION
Washington, D.C. 20590

NOTICE

1. This document is disseminated under the sponsorship of the Department of Transportation in the interest of information exchange. The United States Government assumes no liability for its contents or use thereof.

2. The United States Government and the University of Illinois at Urbana-Champaign do not endorse products or manufacturers. Trade or manufacturers' names appear herein solely because they are considered essential to the object of this report.

Technical Report Documentation Page

1. Report No.	2. Government Accession No.	3. Recipient's Catalog No.
FRA-ORDD 75-7		

4. Title and Subtitle	5. Report Date
CONCRETE FOR TUNNEL LINERS: BEHAVIOR OF STEEL FIBER REINFORCED CONCRETE UNDER COMBINED LOADS	August 1974
	6. Performing Organization Code
7. Author(s) Kenneth S. Herring, John W. Laws, Clyde E. Kesler, Stanley L. Paul, Arthur R. Robinson	8. Performing Organization Report No. UILU-ENG-74-2025
9. Performing Organization Name and Address Department of Civil Engineering University of Illinois at Urbana-Champaign Urbana, Illinois 61801	10. Work Unit No. (TRAIS)
	11. Contract or Grant No. DOT FR 30022
12. Sponsoring Agency Name and Address Federal Railroad Administration Department of Transportation Washington, D. C. 20590	13. Type of Report and Period Covered August 1972-August 1974 Final Report
	14. Sponsoring Agency Code

15. Supplementary Notes

16. Abstract

This study was undertaken to determine the behavior of a steel fiber reinforced concrete member subjected to combined compressive and flexural loads. In addition, information was obtained on the tensile stress-strain relationship, the modulus of elasticity in compression, and Poisson's ratio.

Interaction diagrams are presented for concretes made with two quick setting cements and fiber contents of 0.9, 1.2 and 1.5 percent by volume. Compressive failures, tensile failure, and simultaneous compressive-tensile failures were obtained depending on the moment to axial load ratio.

A method is presented for determining the tensile stress-strain relationship for a length of beam immediately surrounding a crack. This tensile stress-strain relationship makes possible a computerized post-crack analysis of a fiber reinforced concrete structures.

Fiber content, fiber orientation, and type of cement appear to have little affect on Poisson's ratio but do influence the modulus of elasticity and the strength.

17. Key Words	18. Distribution Statement
Steel Fiber Reinforcement, Quick Setting Cement, Combined Loading, Tensile Stress-Strain Relationship, Poisson's Ratio, Modulus of Elasticity, Interaction Diagrams.	Document is available to the public through the National Technical Information Service, Springfield, Virginia 22151

19. Security Classif. (of this report)	20. Security Classif. (of this page)	21. No. of Pages	22. Price
Unclassified	Unclassified	80	

Form DOT F 1700.7 (8-72) Reproduction of completed page authorized

* U. S. GOVERNMENT PRINTING OFFICE : 1973 726-104/223

ACKNOWLEDGEMENT

This study was conducted in the Department of Civil Engineering of the University of Illinois at Urbana-Champaign. The research was supported by the Federal Railroad Administration, Department of Transportation, through contract No. DOT FR 30022, under the technical direction of Mr. William N. Lucke.

TABLE OF CONTENTS

LIST OF TABLES

LIST OF FIGURES

NOMENCLATURE

A	area
a	distance from neutral axis to outer tension fiber
B	y-intercept of log $\lvert\overline{\Delta M}\rvert$ vs. log $\Delta\phi$ graph
b	width of rectangular members
c	distance from neutral axis to outer compression fiber
C	total internal compressive force in concrete
d,h	depth of rectangular member
E_c	Young's Modulus in compression
E_t	Young's Modulus in tension
e	eccentricity with respect to mid-depth of section
Δe	increase in eccentricity due to deflection
f_{cn}, f_{lc}	compressive stress in concrete
f'_r	compressive strength of 4 in. by 8-in. (100 mm by 200-mm) cylinders
f'_r	flexural strength or modulus of rupture of concrete
f_{lt}	tensile stress at the proportional limit
f_{tn}	tensile stress in flexure at the outer fiber

Δf_{tn}	change in tensile stress
h	depth of rectangular member
I	moment of inertia
L	length
M	bending moment
$M_{elastic}$	moment in the elastic region
M_{max}	ultimate bending moment
ΔM	difference between applied and calculated moment
$M'_{elastic}$	initial slope of M-ϕ diagram
$\overline{\Delta M}$	difference between actual moment and the moment found from extrapolation of the original slope of the M-ϕ curve
$\overline{\Delta M}'$	slope change at the discontinuity in the M-ϕ diagram
P	load
P_{max}	ultimate load
ΔP	difference between applied and calculated load
R_n	shift of the neutral axis, when determining the portion of the tensile stress-strain curve after the stress drop
ΔR_n	change in R_n

T	total internal tensile force in concrete
x	distance between stresses used in tensile stress-strain analysis
Z	coordinate axis through the depth of the section
α, β	coefficients relating to magnitude and position of internal compressive force in concrete, as used in the ACI code
ε	strain
$\varepsilon_c, \varepsilon_{cn}$	compressive strain in concrete
$\varepsilon_{c\mu}$	ultimate compressive strain in concrete
$\varepsilon_o, \varepsilon_{pl}$	tensile strain in concrete at first cracking
ε_{tn}	tensile strain in concrete
ν	Poisson's ratio
ϕ	curvature
$\Delta\phi$	curvature measured from slope discontinuity in M-ϕ curve
σ_o, σ_{pl}	tensile stress at the proportional limit corresponding to first cracking
σ_x	stress normal to cross section
σ_{xc}	compressive stress
σ_{xt}	tensile stress
$\Delta\sigma$	tensile stress drop at the proportional limit

CHAPTER 1

INTRODUCTION

1.1 PROBLEMS AND OBJECTIVE

Although some of the first research on concrete reinforced with short pieces of steel was done in 1910[1]* and a British patent was issued in 1914[2], there was little progress in understanding or using fiber reinforced concrete until the early 1960's. The research in the last decade, while significant in many respects, is not sufficient to provide all the information needed for the safe and economical designs of steel-fiber reinforced concrete structures.

The present program was undertaken to obtain the information needed for the analysis and design of a steel-fiber reinforced concrete tunnel lining. The information is, however, applicable to structures in general.

The design of ordinary reinforced concrete beam-columns is ordinarily carried out with the aid of an interaction diagram. This failure envelope provides the designer with the basic information needed to predict loading combinations which can be carried safely by a given member. It would be prohibitively expensive to determine a large number of interaction diagrams experimentally. However, knowledge of the behavior of the concrete and reinforcement in their various regimes of action makes it possible for the engineer to construct interaction diagrams analytically.

---

* Numbers in small type in the text refer to the entries in the list of References.

The present study can be considered as a step in developing information and procedures which will not only permit the engineer to construct interaction diagrams for steel-fiber reinforced concrete members, but also make possible a computerized post-crack analysis of a fiber reinforced concrete structure.

The study consists of several parts. Moment interaction diagrams were found experimentally for small beam-column specimens using two kinds of cement and three different percentages of fiber reinforcement. Compression tests were run using the same variations in material properties, and also different fiber orientations. These tests made it possible to determine the behavior of the material in compression, without considering the effects of strain gradient. Young's modulus, Poisson's ratio, and the general stress-strain characteristics were determined. Since the tensile strength of fiber reinforced concrete is greater than that of plain concrete, and is also more reliable, flexural tests were carried out to determine the tensile behavior of fiber reinforced concrete in a beam. Thus the test program includes both the direct experimental determination of interaction diagrams and information on the behavior and mechanical properties of the material.

1.2 OUTLINE OF TESTS

Standard 6 in. by 12-in. (150 mm by 300-mm) cylinders were used for the determination of a secant Young's Modulus and Poisson's ratio for the steel-fiber reinforced concretes. Concretes made with regulated-set cement and Duracal cement, and having fiber contents of 0.9, 1.2, and 1.5 percent were used. The effect of fiber orientation was also studied.

A total of 19 beam-columns composed of regulated-set cement concrete and 12 beam-columns composed of Duracal cement concrete were tested. An outline of these tests is given in Tables 1.1 and 1.2. The major variables within the two groups were percent of steel fiber reinforcement and eccentricity of load. The beam-columns were all 6 in. (150 mm) square with a total length of 38 in. (965 mm), the prismatic section being 24 in. (610 mm) in length. All beam-columns were tests in 12 to 15 increments of load to failure, the total time of testing ranging between 30 and 45 minutes. Strains on the concrete surface and deflections of the prismatic section were measured at the end of each load increment.

A series of 9 flexural specimens measuring 6 in. by 6 in. by 64 in. (150 mm by 150 mm by 1625 mm), 3 each with fiber contents of 0.9, 1.2 or 1.5 percent by volume made with Duracal cement concrete was tested in pure bending for the determination of the tensile stress-strain behavior. The length of the segment of the beam subject to pure moment was 40 in. (1015 mm). Load was applied continually to failure, while load and deflections of the segment under pure moment were measured electronically.

TABLE 1.1

SUMMARY OF RESULTS OF REGULATED SET CEMENT CONCRETE BEAM-COLUMN TESTS

Specimen	Age at test, days	Fiber content, percent	e, in.(mm)	P, kips(kN)	M, in.-kip (kN•m)	Δe, in.(mm)	Compressive strength, psi (MPa)	Flexural strength, psi(MPa)	ε_{cu}, $x10^{-3}$	Mode of failure*
MI-RS-0.9A	30	0.9	0.0 (0.0)	185.1 (823.4)	5.6 (0.63)	0.03 (0.76)	6160 (42.5)	1030 (7.10)	2.50	C
MI-RS-0.9B	33	0.9	0.50 (12.70)	140.2 (623.6)	81.3 (9.19)	0.08 (2.03)	6160 (42.5)	1030 (7.10)	2.60	C
MI-RS-0.9C	32	0.9	1.75 (44.75)	79.2 (352.3)	148.1 (16.73)	0.12 (3.05)	5830 (40.2)	1090 (7.52)	2.80	CT
MI-RS-0.9D	33	0.9	3.00 (76.20)	20.1 (89.4)	64.7 (7.31)	0.22 (5.59)	6160 (42.5)	1030 (7.10)	--	T
MI-RS-1.2A	29	1.2	0.0 (0.0)	187.0 (831.8)	5.6 (0.63)	0.03 (0.76)	6640 (45.8)	1330 (9.17)	3.20	C
MI-RS-1.2B	35	1.2	0.50 (12.70)	140.5 (625.0)	81.5 (9.21)	0.08 (2.03)	5990 (41.3)	990 (6.83)	2.60	C
MI-RS-1.2C	28	1.2	0.50 (12.70)	164.9 (733.5)	97.3 (10.99)	0.09 (2.29)	7180 (49.5)	960 (6.62)	2.90	C
MI-RS-1.2D	29	1.2	1.00 (25.40)	116.9 (520.0)	128.6 (14.53)	0.10 (2.54)	6170 (42.5)	1080 (7.45)	3.20	C
MI-RS-1.2E	31	1.2	1.50 (38.10)	96.8 (430.6)	157.8 (17.83)	0.13 (3.30)	6690 (46.1)	1130 (7.79)	3.40	C
MI-RS-1.2F	28	1.2	1.75 (44.45)	80.8 (359.4)	154.3 (17.43)	0.16 (4.06)	6630 (45.7)	1080 (7.45)	3.20	CT

(continued)

*C denotes compression failure; CT denotes combined compression and tension failure; and T denotes tension failure.

TABLE 1.1 (CONTINUED)

Specimen	Age at test, days	Fiber content, percent	e, in.(mm)	P, kips(kN)	M, in.-kip (kN•m)	Δe, in.(mm)	Compressive strength, psi (MPa)	Flexural strength, psi(MPa)	ε_{cu}, $x10^{-3}$	Mode of failure*
MI-RS-1.2G	28	1.2	1.75 (44.45)	99.9 (444.4)	196.6 (22.21)	0.22 (5.59)	7120 (49.1)	1130 (7.72)	3.70	CT
MI-RS-1.2H	31	1.2	2.00 (50.80)	67.8 (301.6)	145.8 (16.47)	0.15 (3.81)	5560 (38.3)	1090 (7.52)	--	T
MI-RS-1.2I	31	1.2	2.50 (63.50)	48.2 (214.4)	128.7 (14.54)	0.17 (4.32)	6230 (43.0)	1070 (7.38)	--	T
MI-RS-1.2J	34	1.2	3.00 (76.20)	28.1 (125.0)	90.2 (10.19)	0.21 (5.33)	6180 (42.6)	1250 (8.62)	--	T
MI-RS-1.2K	33	1.2	3.50 (88.90)	18.8 (83.6)	70.5 (7.97)	0.25 (6.35)	6020 (41.5)	1090 (7.52)	--	T
MI-RS-1.5A	28	1.5	0.0 (0.0)	187.0 (831.8)	9.4 (1.06)	0.05 (1.27)	6830 (47.1)	1310 (9.03)	2.50	C
MI-RS-1.5B	32	1.5	0.50 (12.70)	153.4) (682.4)	89.0 (10.06)	0.08 (2.03)	6710 (46.3)	1160 (8.00)	2.40	C
MI-RS-1.5C	32	1.5	1.75 (44.75)	92.5 (411.5)	176.7 (19.96)	0.16 (4.06)	6910 (47.6)	1540 (10.62)	2.80	CT
MI-RS-1.5D	32	1.5	3.00 (76.20)	35.8 (159.2)	114.6 (12.95)	0.20 (5.08)	7420 (51.2)	1150 (7.93)	--	T

*C denotes compression failure; CT denotes combined compression and tension failure; and T denotes tension failure.

TABLE 1.2

SUMMARY OF RESULTS OF DURACAL CEMENT CONCRETE BEAM-COLUMN TESTS

Specimen	Age at test, days	Fiber content, percent	e, in.(mm)	p, kips(kN)	M, in.-kips (kN·m)	Δe, in.(mm)	Compressive strength, psi (MPa)	Flexural strength, psi(MPa)	ε_{cu}, $x10^{-3}$	Mode of failure*
MI-D-0.9A	28	0.9	0.0 (0.0)	90.48 (402.5)	1.27 (0.143)	0.014 (0.36)	3570 (24.6)	642 (4.43)	2.10	C
MI-D-0.9B	28	0.9	9.50 (12.70)	69.40 (308.7)	39.38 (4.449)	0.068 (1.73)	3530 (24.3)	666 (4.59)	2.70	C
MI-D-0.9C	28	0.9	1.75 (44.45)	43.50 (193.5)	80.54 (9.100)	0.102 (2.59)	3540 (24.4)	658 (4.54)	2.10	CT
MI-D-0.9D	28	0.9	3.00 (76.20)	14.31 (63.7)	44.15 (4.988)	0.085 (2.16)	3560 (24.6)	585 (4.03)	---	T
MI-D-1.2A	28	1.2	0.0 (0.0)	93.70 (416.8)	1.69 (0.191)	0.018 (0.46)	4010 (27.7)	723 (4.98)	1.70	C
MI-D-1.2B	28	1.2	0.50 (12.70)	74.77 (332.6)	43.67 (4.934)	0.084 (2.13)	3680 (25.4)	772 (5.32)	2.50	C
MI-D-1.2C	28	1.2	1.75 (44.45)	41.48 (184.5)	77.51 (8.757)	0.121 (3.07)	3830 (26.4)	823 (5.67)	2.60	CT
MI-D-1.2D	28	1.2	3.00 (76.20)	17.48 (77.8)	53.91 (6.091)	0.086 (2.18)	3780 (26.1)	896 (6.18)	--	T
MI-D-1.5A	28	1.5	0.0 (0.0)	90.45 (402.3)	1.56 (0.176)	0.001 (0.03)	3970 (27.4)	984 (6.78)	1.70	C

*C denotes a compression failure; CT denotes a combined tension and compression failure and T denotes a tension failure.

(continued)

TABLE 1.2 (CONTINUED)

Specimen	Age at test, days	Fiber content, percent	e, in.(mm)	p, kips(kN)	M, in.-kips (kN·m)	Δe, in.(mm)	Compressive strength, psi (MPa)	Flexural strength, psi(MPa)	ε_{cu}, $x10^{-3}$	Mode of failure*
MI-D-1.5B	28	1.5	0.50 (12.70)	77.89 (346.5)	44.09 (5.981)	0.066 (1.68)	3940 (27.2)	921 (6.35)	2.40	C
MI-D-1.5C	28	1.5	1.75 (44.45)	44.49 (197.9)	83.82 (9.470)	0.134 (3.40)	3880 (26.8)	885 (6.10)	2.70	CT
MI-D-1.5D	28	1.5	3.00 (76.20)	20.39 (90.7)	63.27 (7.149)	0.103 (2.62)	3840 (26.5)	942 (6.49)	--	T

*C denotes a compression failure; CT denotes a combined tension and compression failure and T denotes a tension failure.

CHAPTER 2

MATERIALS AND FABRICATION

2.1 CEMENT

The regulated-set cement was purchased in one lot from the Huron Cement Company and the Duracal cement was purchased in one lot from U. S. Gypsum. Both cements were stored under proper conditions.

2.2 AGGREGATES

The aggregates used in the studies were naturally occurring siliceous sands and gravels from the Wisconsin glaciation period. The gradation and physical properties are given in Tables 2.1 and 2.2.

2.3 FIBERS

The fibers used in all tests were steel fibers milled from thin plates. They were 1 in. (25 mm) long with a cross section of 0.010 in. by 0.022 in. (0.25 mm by 0.56 mm). The fibers were produced by the United States Steel Corporation.

2.4 ADMIXTURES

Citric acid was used in the regulated-set cement concrete mixes to control the setting time. While the purpose for adding the citric acid was to increase the setting time and thus increase the handling time for the mix, it also entrained some air and decreased the water requirement. Since the citric acid did not provide sufficient retardation, the water temperature was lowered to 32 F (0 C) to provide additional retardation.

TABLE 2.1

SIEVE ANALYSIS - SAND AND PEA GRAVEL

Sieve	Sand, percentage		Pea gravel, percentage	
	Retained	Passing	Retained	Passing
3/8-in.	0	100	1	99
No. 4	4	96	94	6
No. 8	12	88	99	1
No. 16	22	78	100	0
No. 30	40	60	100	0
No. 50	84	16	100	0
No. 100	99	1	100	0
No. 200	99	1	100	0
Fineness modulus	2.61		5.93	

TABLE 2.2

PROPERTIES OF SAND AND PEA GRAVEL

Property	Sand	Pea gravel
Unit weight, lb/cu ft (kg/m^3)	107.6 (1724)	100.6 (1612)
Bulk specific gravity, SSD	2.60	2.66
Absorption capacity, percent	2.2	2.2

No admixture was used in the Duracal cement concrete. This cement is prepared at the factory with the necessary additives for the required setting time.

2.5 REINFORCING STEEL

Deformed bars, 3/8 in. (9.5 mm) in size, were used to make reinforcing cages for the capitals of the beam-columns. The bars exceeded the requirements of ASTM designation A615[3] for Grade 60 steel.

2.6 MIX DESIGNS

The concrete mixes employed in this study are shown in Table 2.3. Three different mixes were used for both the regulated-set cement and the Duracal cement concretes. These were designed mainly to vary the fiber content. In general, to maintain proper workability, the paste content had to be increased as the fiber content of the mix increased.

2.7 MIXING PROCEDURE

The concrete was mixed in a 2.5 cu ft (0.071 m^3) capacity, non-tilting drum mixer. First, the aggregates were placed in the mixer and the fibers were added slowly to insure a good fiber distribution. The water and cement were then added and the concrete was mixed throughly.

TABLE 2.3

MIXES FOR FIBER REINFORCED CONCRETE

Mix no.	Water-cement ratio	Mix materials, lb/cu yd					Fiber,[2] percent	Citric acid, lb	Entr'd air, percent	Unit weight wet, lb/cu ft
		Water	Cement	Sand[1]	Pea gravel[1]	Steel fiber				
RS0.9	0.50	325	650	1610	1130	120	0.9	2.0	4.1	142.8
RS1.2	0.45	326	725	1610	1080	160	1.2	1.75	3.7	143.8
RS1.5	0.45	360	800	1670	870	200	1.5	1.65	3.5	144.0
DC0.9	0.36	232	650	1640	1165	120	0.9	--	5.7	142.4
DC1.2	0.36	259	725	1610	1120	160	1.2	--	4.3	144.0
DC1.5	0.35	280	800	1580	1075	200	1.5	--	4.8	145.0

[1] Saturated, surface dry

[2] Percent by volume

TABLE 2.3-SI

MIXES FOR FIBER REINFORCED CONCRETE

Mix no.	Water-cement ratio	Mix materials, kg/m^3					Fiber,[2] percent	Citric acid, g	Entr'd air percent	Unit weight wet, kg/m^3
		Water	Cement	Sand[1]	Pea gravel[1]	Steel fiber				
RS0.9	0.50	193	386	955	670	71	0.9	900	4.1	2314
RS1.2	0.45	194	430	955	640	95	1.2	800	3.7	2307
RS1.5	0.45	214	474	991	516	118	1.5	750	3.5	2278
DC0.9	0.36	137	386	973	691	71	0.9	--	5.7	2281
DC1.2	0.36	154	430	955	664	95	1.2	--	4.3	2307
DC1.5	0.36	156	474	938	638	118	1.5	--	4.8	2323

[1] Saturated, surface dry

[2] Percent by volume

CHAPTER 3

DETAILS OF RESEARCH PROGRAM

3.1 DESCRIPTION AND FABRICATION OF SPECIMENS

3.1.1 SPECIMENS FOR DETERMINING POISSON'S RATIO AND YOUNG'S MODULUS

Six 6 in. by 12-in (150 mm by 300-mm) cylinders and three 3 in. by 3 in. by 15-in. (75 mm by 75 mm by 380-mm) flexural specimens were cast for fiber contents of 0.9, 1.2, and 1.5 percent, using both the regulated-set and Duracal cement concrete mixes, for the study of Poisson's ratio and Young's Modulus.

Within each set of six cylinders, three were vibrated externally and parallel to the longitudinal axis and three were vibrated externally and perpendicular to the longitudinal axis. The two directions of vibration were used to obtain the two extreme cases of fiber orientation that might be found in a typical fiber reinforced concrete structure.

In the cylinders which were vibrated parallel to the longitudinal axis, the fibers tended to be oriented perpendicular to the longitudinal axis of the cylinder; and in those cylinders vibrated perpendicular to the longitudinal axis, the fibers tended to be oriented parallel to the longitudinal axis of the cylinder.[4] This phenomenon is a result of the tendency of a long, thin body suspended in a liquid medium to orient itself perpendicular to the direction of wave motion.

3.1.2 BEAM-COLUMN SPECIMENS

The beam-column specimens were made short to eliminate the possibility of buckling failure. The details of the specimen are shown in Fig. 3.1. The light reinforcement cages in the capitals of the beam-columns were sufficient to insure that failure of the specimens under load took place in the prismatic section.

The regulated-set cement concrete beam-columns, except for specimens MI-RS-1.2C and MI-RS-1.2G, were cast in a wooden form in a horizontal position and vibrated internally. All of the Duracal cement specimens, MI-RS-1.2C, and MI-RS-1.2G were cast in a steel form in a horizontal position and vibrated externally. The use of the steel form, instead of the wooden form, reduced the variation in lateral dimensions of the prismatic section from $\pm$ 0.10 in. (2.5 mm) to $\pm$ 0.03 in. (0.8 mm).

Internal vibration was suspected of disturbing the fiber distribution at the points of vibration and thus adversely affecting the strength. To check this hypothesis, specimens MI-RS-1.2C and MI-RS-1.2G were vibrated externally so that their test results could be compared with those of corresponding specimens which were vibrated internally.

Along with each beam-column specimen, three 4 in. by 8-in. (100 mm by 200-mm) cylinders and three 3 in. by 3 in. by 15-in. (75 mm by 75 mm by 380-mm) flexural specimens were cast as controls.

3.1.3 FLEXURAL SPECIMENS FOR TENSILE STRESS-STRAIN CURVE DETERMINATION

A set of three 6 in. by 6 in. by 64-in. (150 mm by 150 mm by 1625 mm) flexural specimens was cast with fiber contents of 0.9, 1.2, and

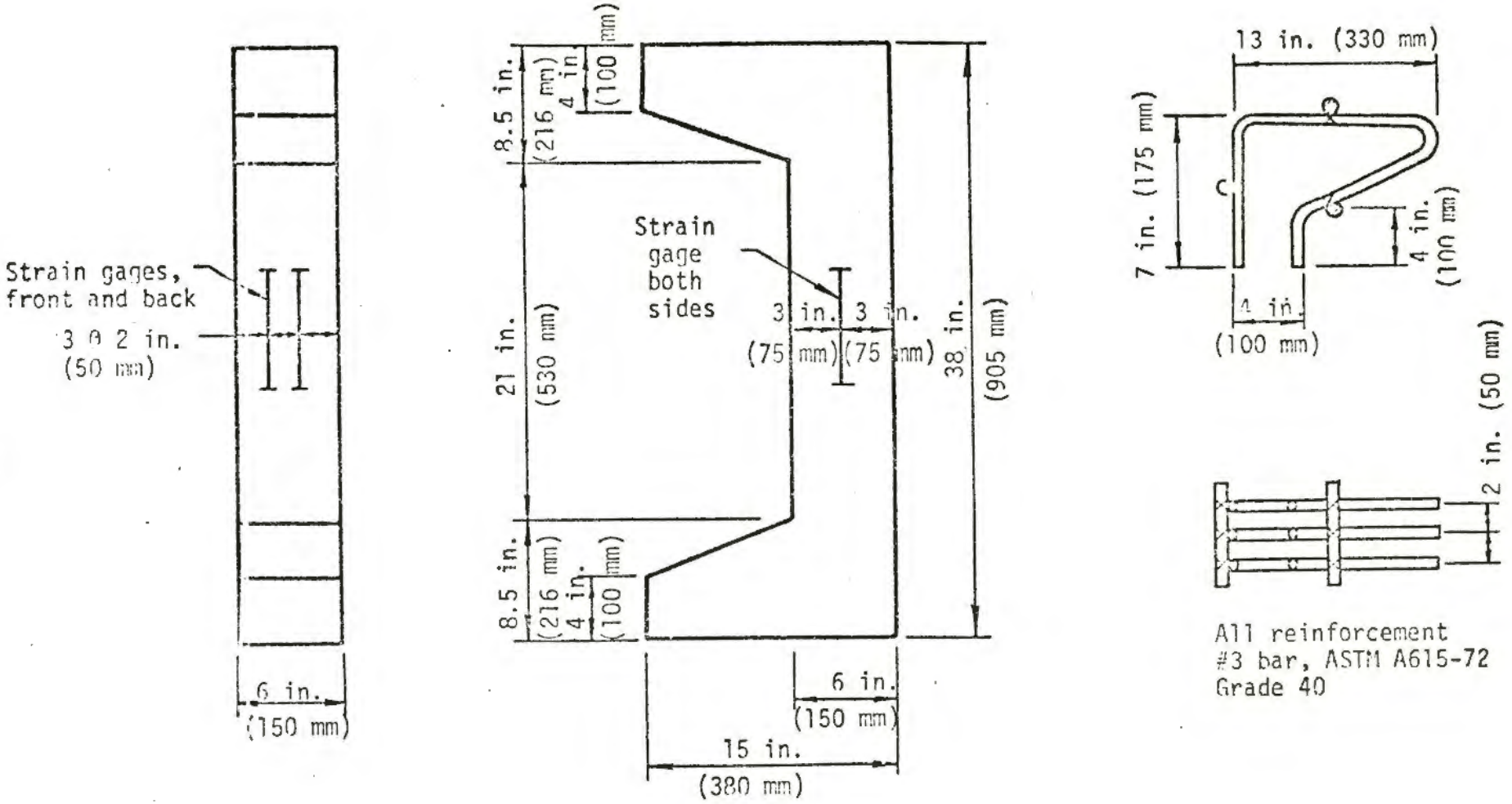

FIG. 3.1 DETAILS OF BEAM-COLUMN AND CAPITAL REINFORCEMENT

1.5 percents using Duracal cement concrete. These were cast in a horizontal position and vibrated externally. The lateral dimensions of the specimen were within a tolerance of ± 0.05 in. (1.3 mm).

Three 4 in. by 8-in. (100 mm by 200-mm) cylinders and three 3 in. by 3 in. by 15-in. (75 mm by 75 mm by 380-mm) flexural specimens were cast with each set of large beams to serve as controls.

3.2 CURING PROCEDURE

After casting, all specimens were placed in a fog room at a temperature of 75 to 80 F (24 to 27 C) for a period of 21 days. They were then removed and stored in a laboratory environment until testing, during which time electric strain gages were mounted where needed.

3.3 INSTRUMENTATION

The apparatus used for measurement of the longitudinal and lateral strains on the cylinders for the determination of Young's Modulus and Poisson's ratio is shown in Figs. 3.2 and 3.3.

The compressometer for the measurement of longitudinal strains is shown in Fig.3.2. This device consists of two rings, one fixed to the cylinder and one free to rotate about fixed points on the cylinder while pivoting on a rigid rod attached to the fixed ring. Directly opposite the fixed rod, at the same distance from the points of ring rotation as the rod, is a deflection measuring transducer which records the relative deflection of the rings over a 6-in. (150-mm) gage length.

The unbonded gage used for measurement of lateral strains is shown in Fig.3.3. This device consists of a steel band with a gap in it, resting

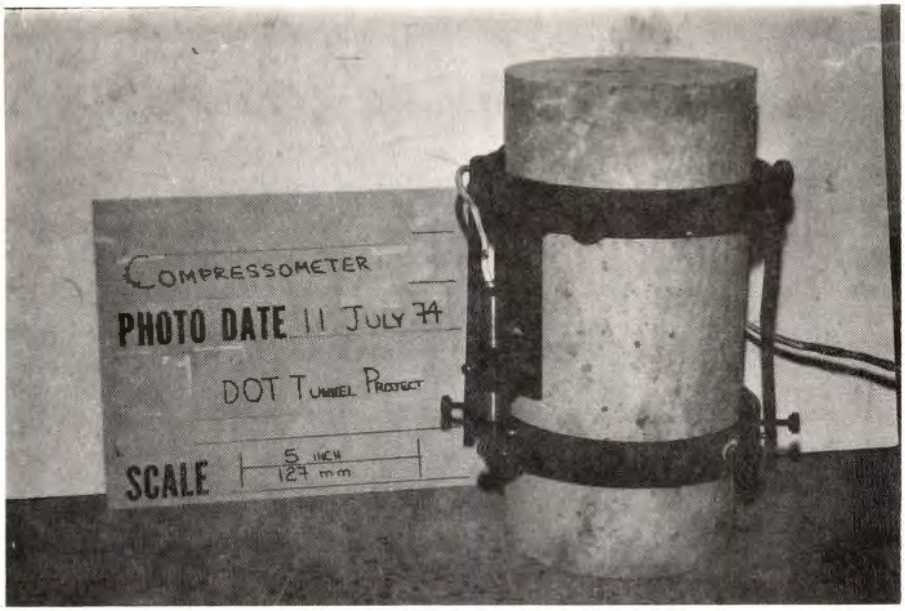

FIG. 3.2 COMPRESSOMETER

FIG. 3.3 UNBONDED LATERAL STRAIN CAGE

against the cylinder on a series of rollers. As load was applied to a specimen, the change of the width of the gap was measured using a transducer to give the change in circumference of the specimen.

The readings of the above instruments were continuously recorded and plotted against load on X-Y plotters.

A beam-column undergoing test is shown in Fig. 3.4. Strains on the surface of the beam-columns were measured using electric strain gages with a 6-in. (152-mm) gage length, which were attached to a portable strain indicator. The arrangement of the strain gages is indicated in Fig. 3.1. The 6-in. (152-mm) gage length was chosen to give the strains over a sufficiently long gage length to average out irregular strains, such as might be caused by the aggregate particles. This length was suitable since the coarse aggregate was 3/8-in. (10-mm) pea gravel. Dial indicators with a 4-in. (100-mm) travel were used to measure the deflections of the prismatic section of the beam-columns.

The 6 in. by 6 in. by 64-in. (150 mm by 150 mm by 1625-mm) flexural specimens were tested in pure bending, Fig. 3.5, using a very stiff loading apparatus and a 600,000 lb (2.67 MN) capacity hydraulic testing machine. The deflections and storage of energy in the loading apparatus during the test were thus minimized so that effects of the stiffness of the testing apparatus on the recorded behavior of the test specimens were negligible. The total span length was 60 in. (1525 mm), and the central portion subject to pure moment was 40 in. (1015 mm) in length. Deflections of the beam were measured using transducers. These deflections were continuously plotted against load on X-Y plotters.

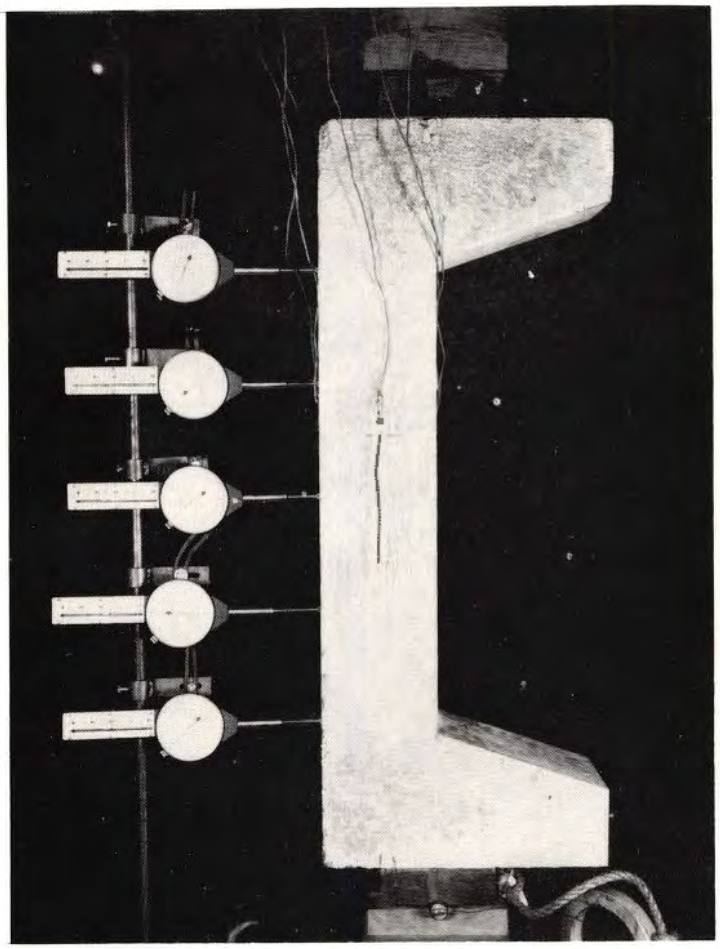

FIG. 3.4 BEAM-COLUMN UNDER TEST

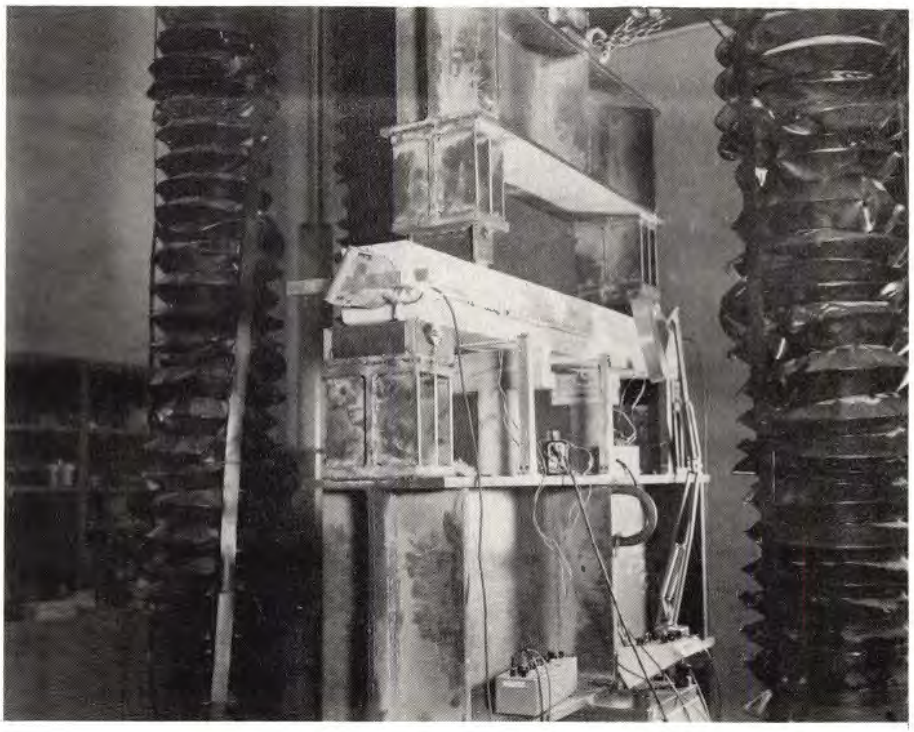

FIG. 3.5 LARGE FLEXURAL SPECIMEN UNDER TEST

All specimens were tested in hydraulic machines of appropriate capacity.

3.4 TESTING PROCEDURE

3.4.1 CONTROL SPECIMENS

The 3 in. by 3 in. by 15-in. (75 mm by 75 mm by 380-mm) flexural specimens were tested with a third-point loading according to ASTM designation C78[5] for the determination of the modulus of rupture. The 4 in. by 8-in. (100 mm by 200-mm) cylinders, used to determine compressive strengths, were tested according to ASTM designation C39.[6]

3.4.2 POISSON'S RATIO AND YOUNG'S MODULUS SPECIMENS

The 6 in. by 12-in. (150 mm by 300-mm) cylinders were tested in uniaxial compression in accordance with ASTM designation C469,[7] except that they were loaded at a constant longitudinal strain rate of 0.0025/min. Load was applied continuously to failure.

3.4.3 BEAM-COLUMN SPECIMEN

Load was applied to the beam-column specimens through cylindrical bearings. All specimens were loaded at a constant crosshead rate of 0.03 in./min (0.8 mm/min). An average of the readings of each pair of strain gages on the compression, center and tension faces of the cross section was recorded to give an indication of the strain distribution across the cross section of the specimen in the plane of loading. Deflections of the prismatic section

were recorded so that an accurate value of the moment could be determined at each stage of loading. A specimen undergoing test is shown in Fig. 3.4.

The specimens were carefully balanced and centered in the testing machine. Initial readings of all strain gages and dial indicators were taken with a preload of 300 lb (1334 N). This was later taken into account by plotting all readings against load and extrapolating the graphs to zero load to determine the change in initial readings due to the preload. Load was then applied to each specimen in 12 to 15 increments to failure, with readings of all instrumentation being taken at the end of each increment.

Since it was impossible to take readings at failure, all graphs of instrument readings were extrapolated to the failure load to determine the values of strains and deflections corresponding to failure.

3.4.4 FLEXURAL SPECIMENS FOR THE DETERMINATION OF THE TENSILE STRESS-STRAIN RELATION

A 6 in. by 6 in. by 64-in. (150 mm by 150 mm by 1625-mm) flexural specimen is shown in Fig. 3.5 as it is being tested. The specimens were loaded at a constant crosshead rate of 0.03 in./min (0.8 mm/min). The bottom portion of the loading apparatus was bolted to the base of the testing machine and load was applied to the top portion through a spherical bearing.

The deflections of the beam were measured at the center and 18 in. (0.457 m) either side of the center. The difference of the center deflection and the average of the two outer deflections was recorded during the test. Thus, only the deflection of a 36-in. (914-mm) portion of the beam under pure moment was used for analysis. This was done in order to minimize the

effects of the disturbance of the stress distribution near the points of application of the load on the behavior of the beam segment. The load was applied continuously until failure of the specimen.

CHAPTER 4

EXPERIMENTAL RESULTS

4.1 POISSON'S RATIO AND YOUNG'S MODULUS IN COMPRESSION

The resulting values of Poisson's ratio, ν, and the secant Young's Modulus in compression, E_c, for the various mixes and directions of vibration are shown in Table 6. These values were computed according to ASTM designation C-469.[7] Each value indicated in Table 4.1 is an average of three separate cylinder tests.

The results indicate that Poisson's ratio did not seem to be influenced by any of the variables and that the value for the concrete mixes used here may be taken as 0.14 ± 0.02.

The values of the secant Young's modulus in compression, on the other hand, show a definite dependence on both the fiber orientation and type of concrete used. The value of E_c is higher for the regulated-set cement concrete than for the Duracal cement concrete when comparing corresponding fiber contents and orientations. That is, regulated-set cement paste is stiffer than the Duracal cement paste. The values of E_c within a given batch of concrete were consistently higher in the cylinders in which the general fiber orientation was parallel to, rather than perpendicular to, the longitudinal axis. This is due to the large difference between the Young's Modulus of the concrete matrix and that of the steel fibers. The more fibers that tend to be oriented parallel to the direction of stress, the greater the effect they will have on increasing Young's Modulus of the composite material.

The compressive strengths in the cylinders with the fiber orientation

TABLE 4.1

COMPRESSIVE YOUNG'S MODULUS AND POISSON'S RATIO FOR DURACAL AND REGULATED-SET CEMENT CONCRETES

Fiber content, percent	Cement	Preferred direction of orientation[1]	f_c', ksi (MPa)	f_r', ksi (MPa)	E_c, $x10^3$ksi(GPa)	ν,
0.9	Duracal	Parallel	3.40 (23.4)	0.777 (5.36)	3.37 (23.2)	0.14
		Perpendicular	4.04 (27.9)		3.04 (21.0)	0.14
1.2	Duracal	Parallel	3.84 (26.5)	1.008 (6.95)	3.13 (21.6)	0.12
		Perpendicular	4.19 (28.9)		2.93 (20.2)	0.12
1.5	Duracal	Parallel	3.87 (26.7)	0.951 (6.56)	3.23 (22.3)	0.16
		Perpendicular	4.21 (29.0)		2.96 (20.4)	0.15
0.9	Reg-set	Parallel	5.61 (38.7)	0.875 (6.03)	3.53 (24.3)	0.12
		Perpendicular	6.46 (44.5)		3.06 (21.1)	0.11
1.2	Reg-set	Parallel	6.57 (45.3)	1.080 (7.45)	3.82 (26.3)	0.16
		Perpendicular	7.25 (50.0)		3.47 (23.9)	0.15
1.5	Reg-set	Parallel	6.39 (44.1)	1.110 (7.65)	3.68 (25.4)	0.16
		Perpendicular	6.87 (47.4)		3.19 (22.0)	0.12

[1] Orientation is given with respect to the longitudinal axis of the cylinder.

perpendicular to the longitudinal axis were greater than those in the cylinders with the fiber orientation parallel to the longitudinal axis. The effect of fiber orientation on compressive strength is opposite to the effect of orientation on Young's Modulus, since if the fibers tend to be oriented primarily perpendicular to the longitudinal axis of the cylinder, there will be a greater percentage of the fibers effective in restraining lateral expansion of the cylinder. This, in turn, would lead to a higher ultimate compressive strength, since the splitting of the concrete would require a higher level of stress.

4.2 BEHAVIOR UNDER COMBINED FLEXURAL AND COMPRESSIVE LOADS

The moment-interaction and load-curvature diagrams at ultimate for regulated-set cement concrete and Duracal cement concrete, with fiber contents of 0.9, 1.2, and 1.5 percent, are shown in Figs. 4.1 through 4.6. The points corresponding to zero axial load on the interaction diagrams for Duracal cement concrete were obtained from the tests of the large flexural specimens for the determination of the tensile stress-strain behavior. A summary of the beam-column test results is given in Tables 3.1 and 3.2.

The measured strain distributions across the cross section of each of the specimens at failure are indicated on the interaction diagrams. These values of strain were obtained from the strain gage readings taken at the center of the prismatic section of the beam-columns. The curvatures at failure were obtained from these strain distributions and are plotted against ultimate load in Figs. 4.1 through 4.6.

The resulting strain distributions up to failure indicate that it is reasonable to assume linear variation of strain across the cross section.

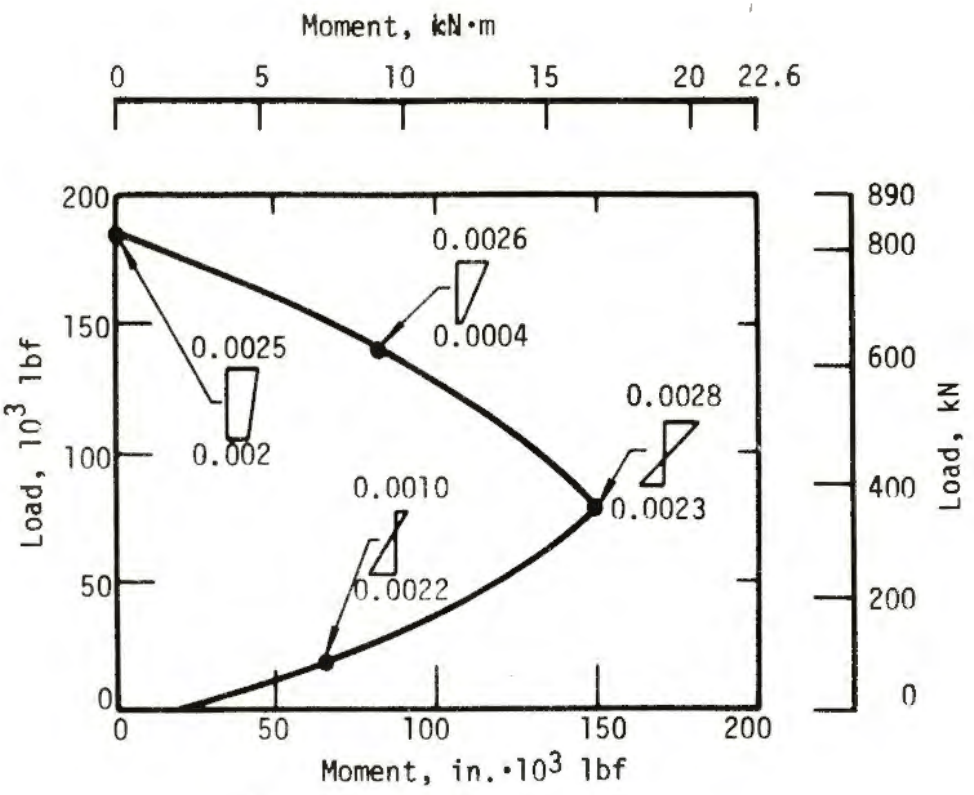

(a) Interaction diagram

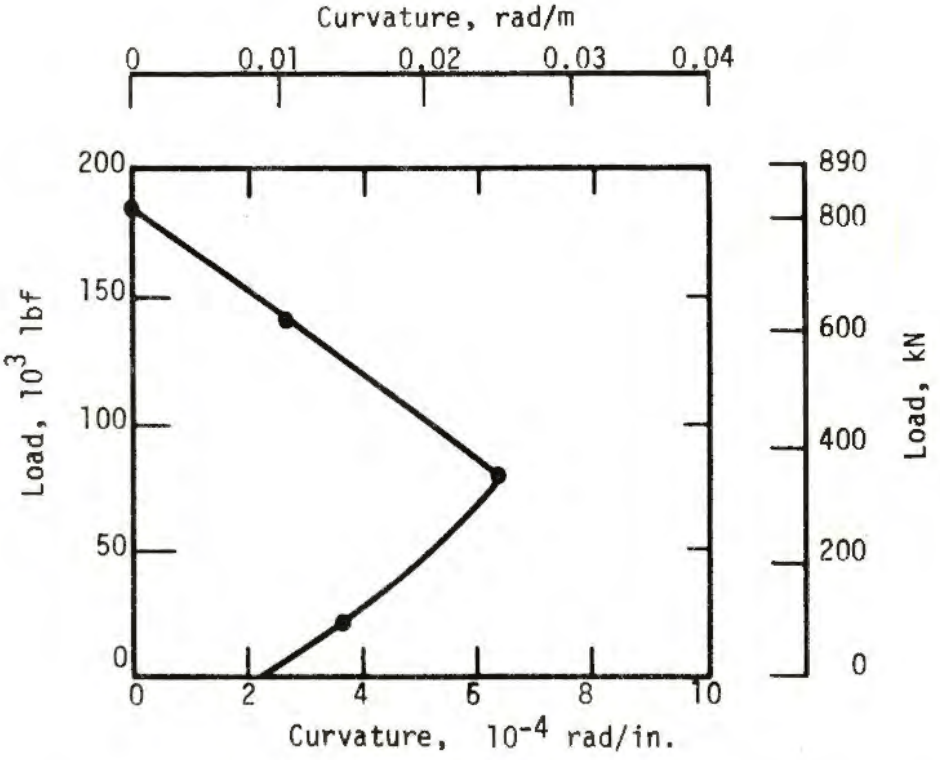

(b) Load-curvature diagram

FIG. 4.1 ULTIMATE INTERACTION AND LOAD-CURVATURE DIAGRAMS FOR 0.9 PERCENT FIBER: REGULATED-SET CEMENT CONCRETE

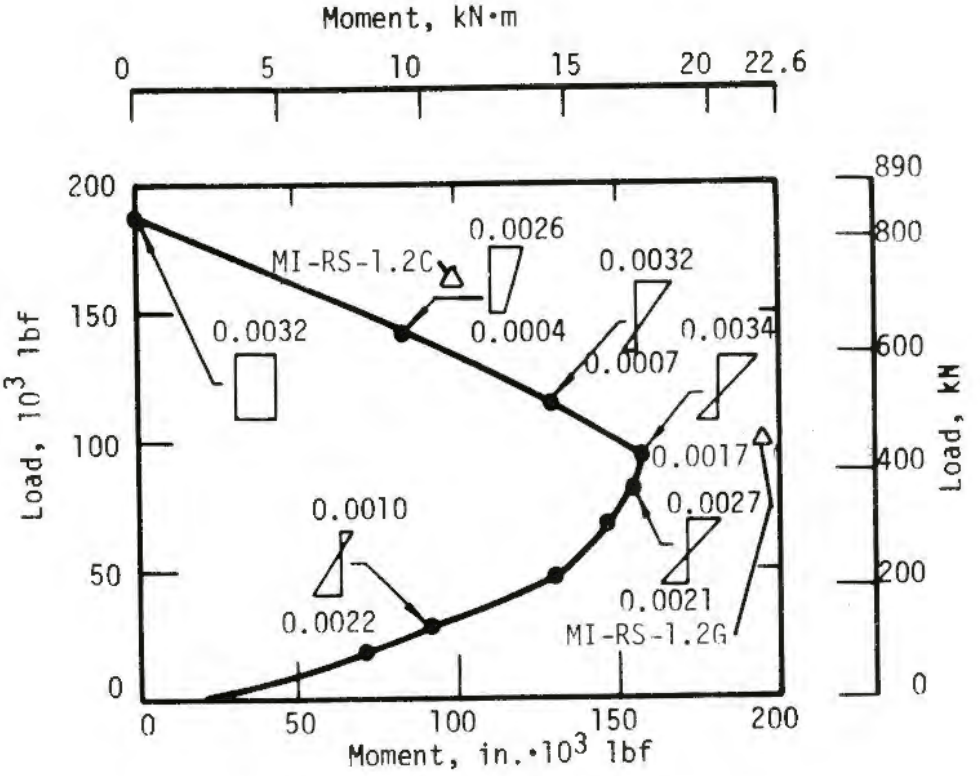

(a) Interaction diagram

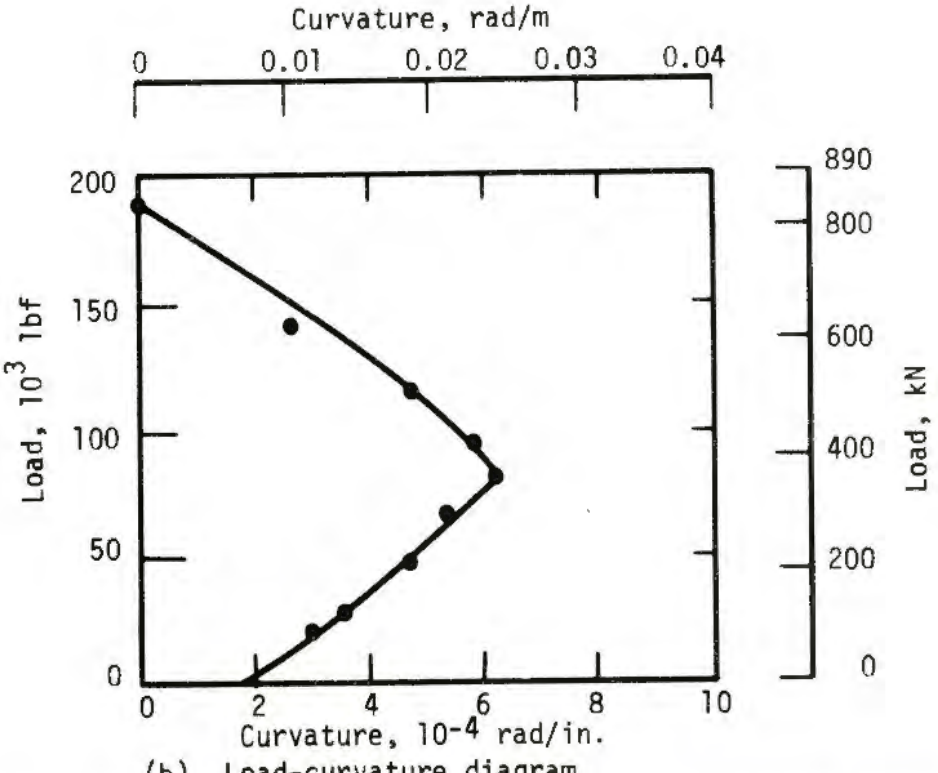

(b) Load-curvature diagram

FIG. 4.2 ULTIMATE INTERACTION AND LOAD-CURVATURE DIAGRAMS FOR 1.2 PERCENT FIBER: REGULATED-SET CEMENT CONCRETE

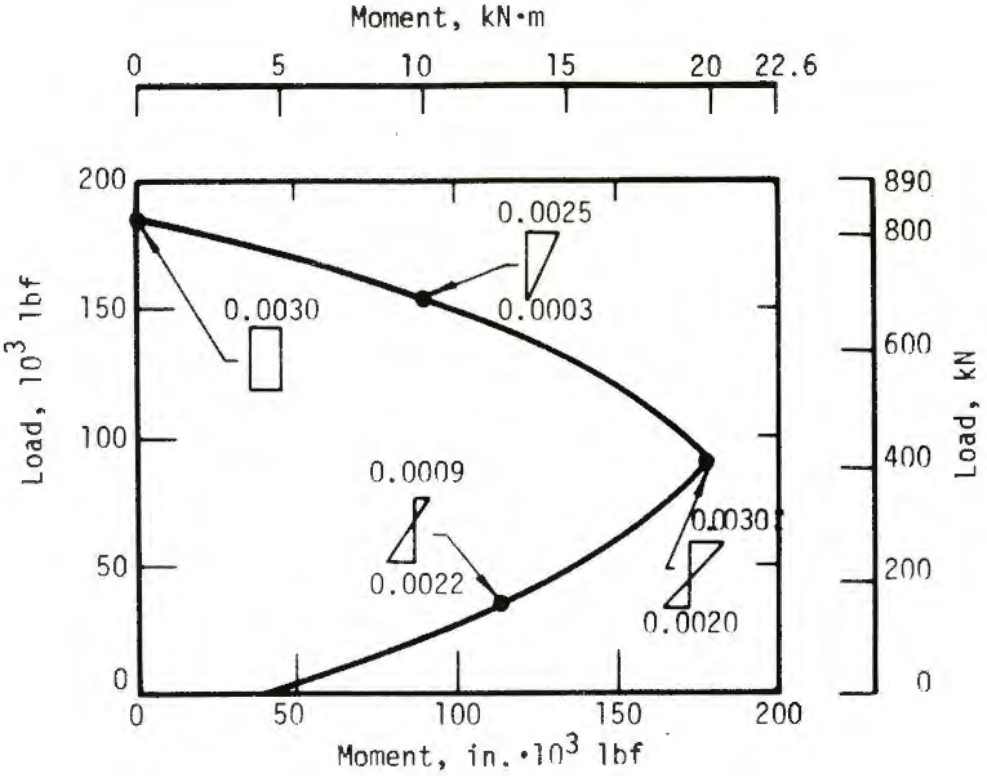

(a) Interaction diagram

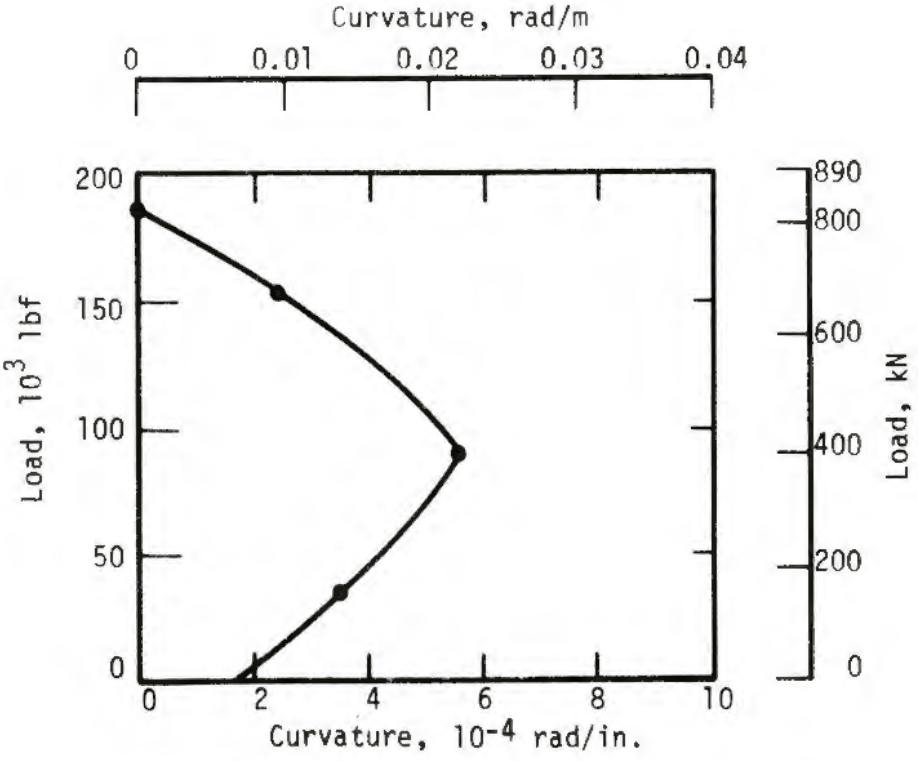

(b) Load-curvature diagram

FIG. 4.3 ULTIMATE INTERACTION AND LOAD-CURVATURE DIAGRAMS FOR 1.5 PERCENT FIBER: REGULATED-SET CEMENT CONCRETE

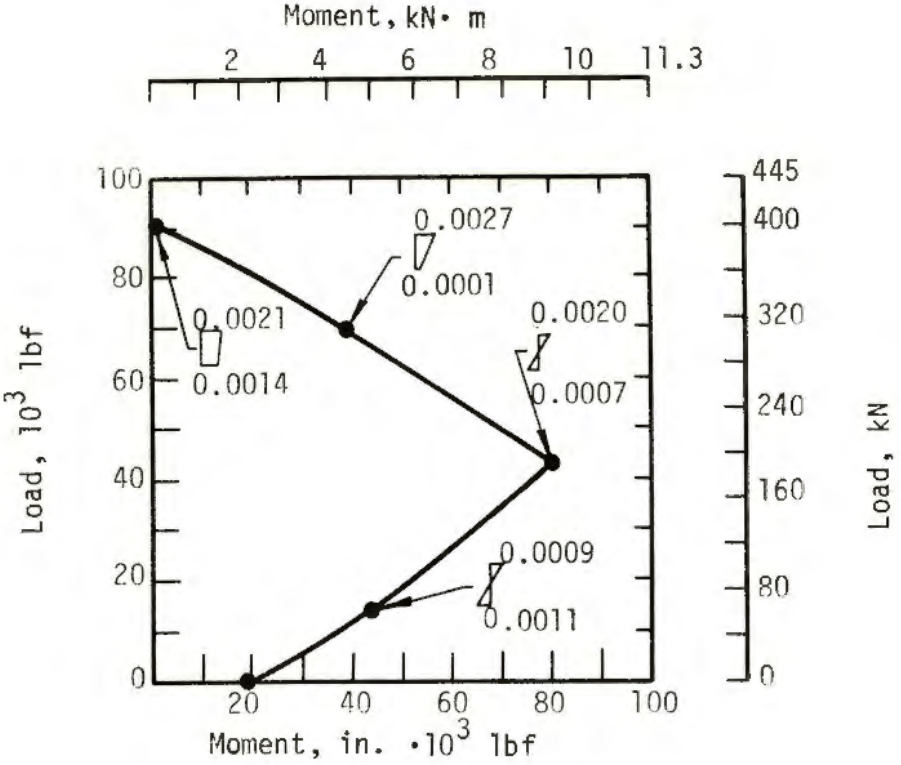

(a) Interaction diagram

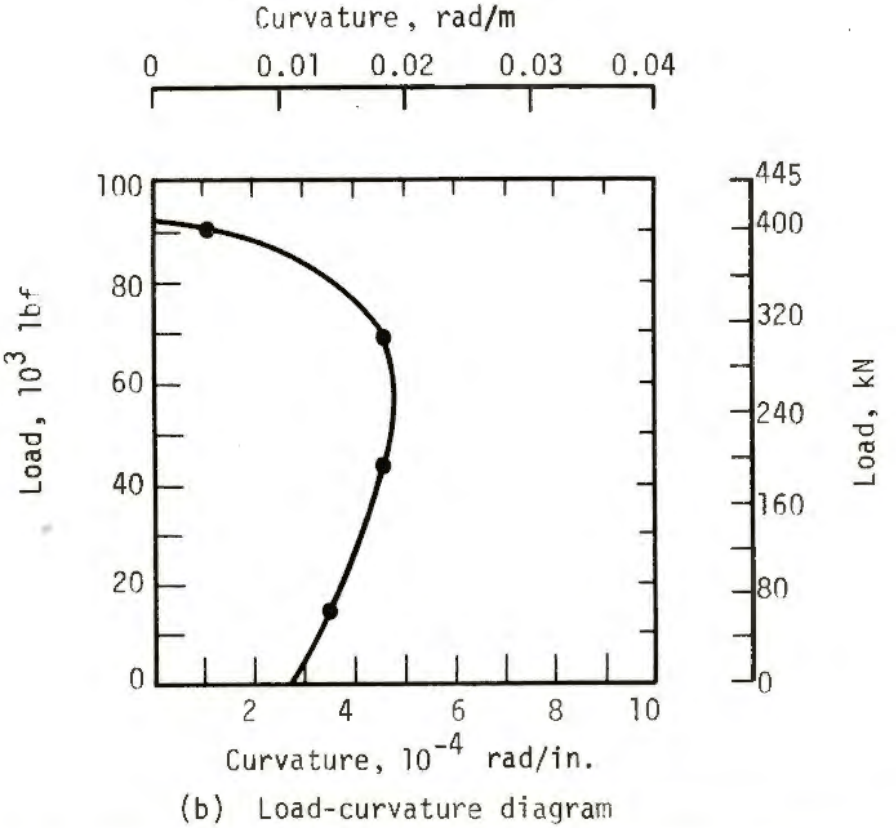

(b) Load-curvature diagram

FIG. 4.4 ULTIMATE INTERACTION AND LOAD-CURVATURE DIAGRAMS FOR 0.9 PERCENT FIBER: DURACAL CEMENT CONCRETE

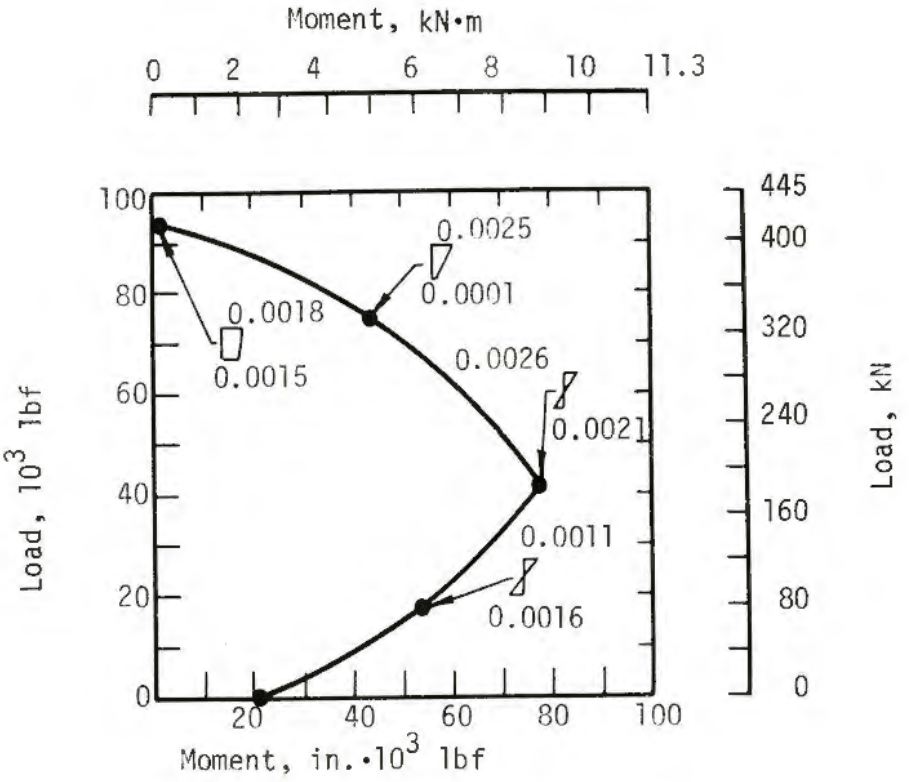

(a) Interaction diagram

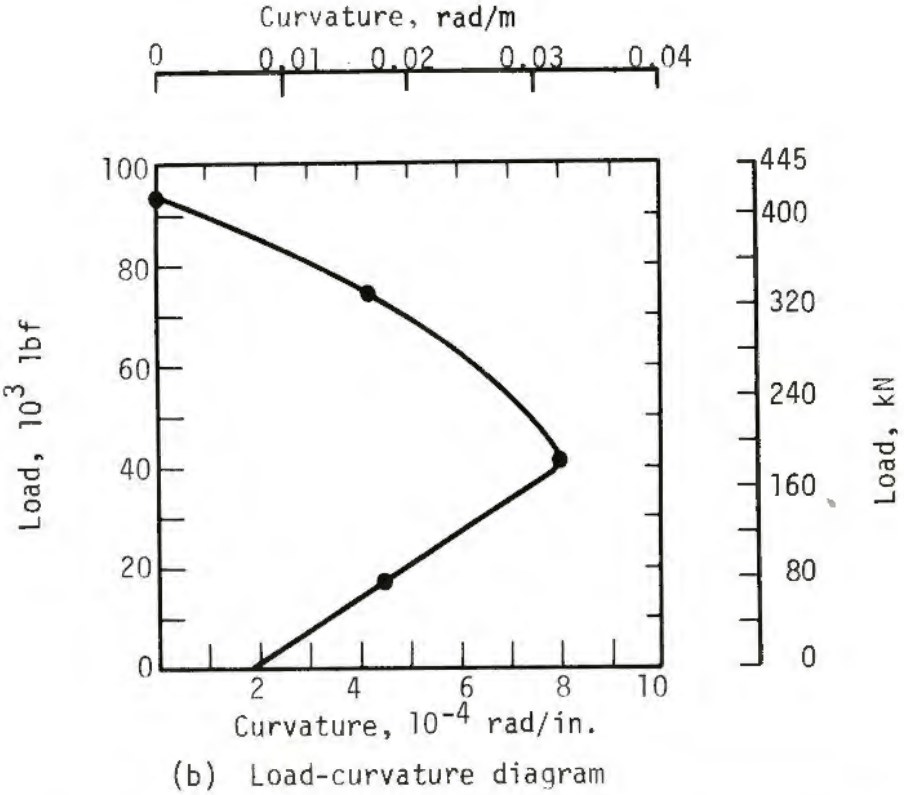

(b) Load-curvature diagram

Fig. 4.5 ULTIMATE INTERACTION AND LOAD-CURVATURE DIAGRAMS FOR 1.2 PERCENT FIBER: DURACAL CEMENT CONCRETE

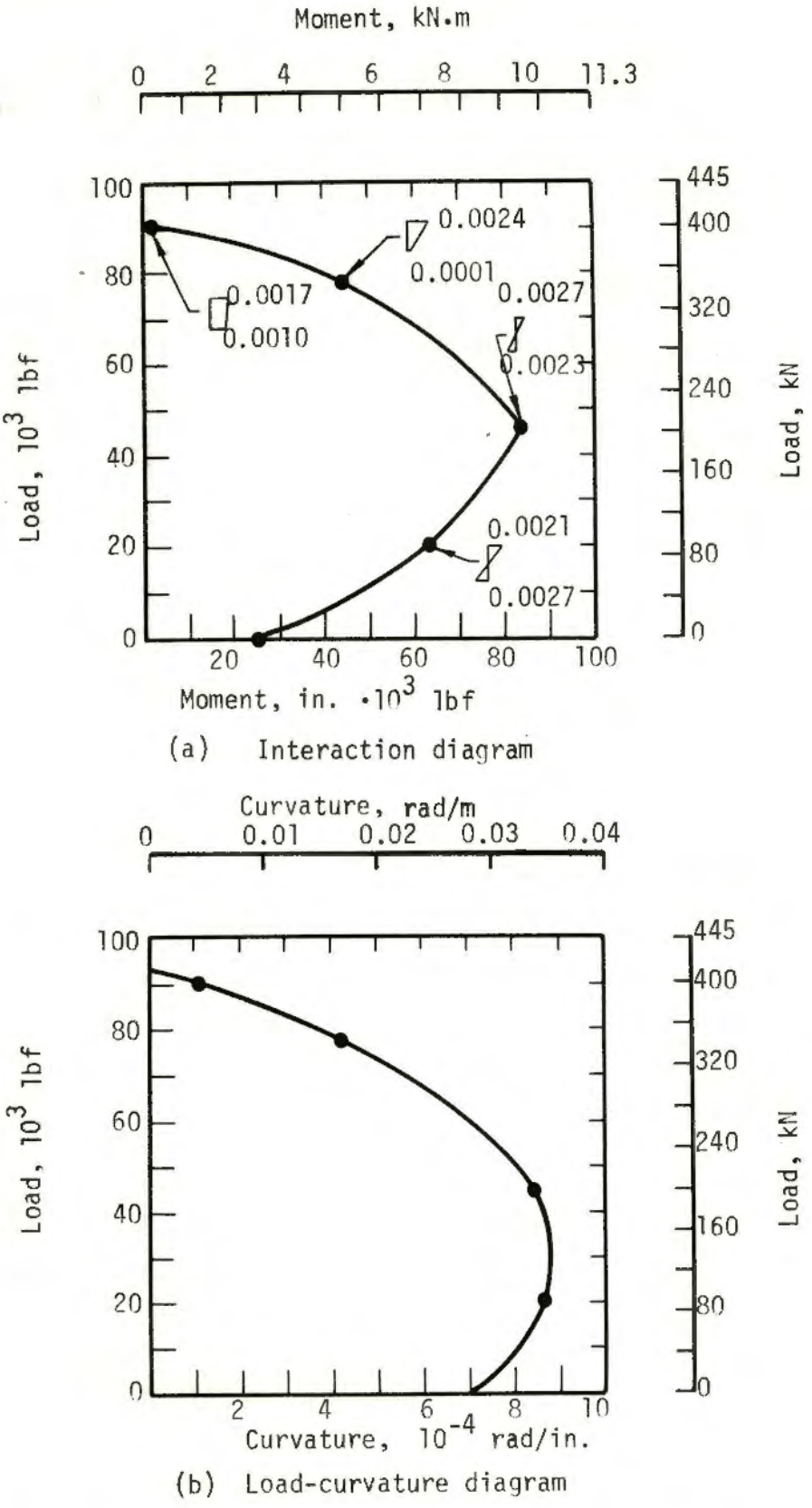

FIG. 4.6 ULTIMATE INTERACTION AND LOAD-CURVATURE DIAGRAMS FOR 1.5 PERCENT FIBER: DURACAL CEMENT CONCRETE

Typical distributions of strain on the cross section at ultimate are shown in Fig. 12 for the 0.9 percent fiber content Duracal cement concrete beam-column.

The series of beam-columns made with regulated-set cement concrete and having a 1.2 percent fiber content was used to determine the general behavior characteristic of the various segments of the moment-interaction diagrams. They were also used to determine at what eccentricity the knee of the interaction diagram occurred in order to facilitate the determination of the entire failure envelope by testing specimens at only four different eccentricities. The initial eccentricities, e, that define the failure envelope were found to be 0.0 in. (0.0 mm), 0.50 in. (12.7 mm), 1.75 in. (44.5 mm) and 3.0 in. (76.2 mm). The knee of the interaction curve was found to be defined by e = 1.75 in. (44.5 mm).

The mode of failure of each specimen is shown in Tables 1.1 and 1.2. Those specimens loaded at small eccentricities, up to about 0.25 d, failed by crushing of the concrete, and are termed compression failures. These failures were somewhat less brittle than those for a conventional reinforced concrete member, due to the restraint which the fibers impose on the crumbling of the concrete. At eccentricities of about 0.25 d to 0.33 d, failure of the specimens was caused by almost simultaneous crushing of the concrete on the compression face and tensile cracking on the tension face which propagated to a point on the cross section near the neutral axis, which was near the central portion of the cross section. This type of failure is termed a combination compression and tension failure. Specimens loaded at eccentricities higher than 0.33 d failed in the tensile cracking on the tension face with no spalling

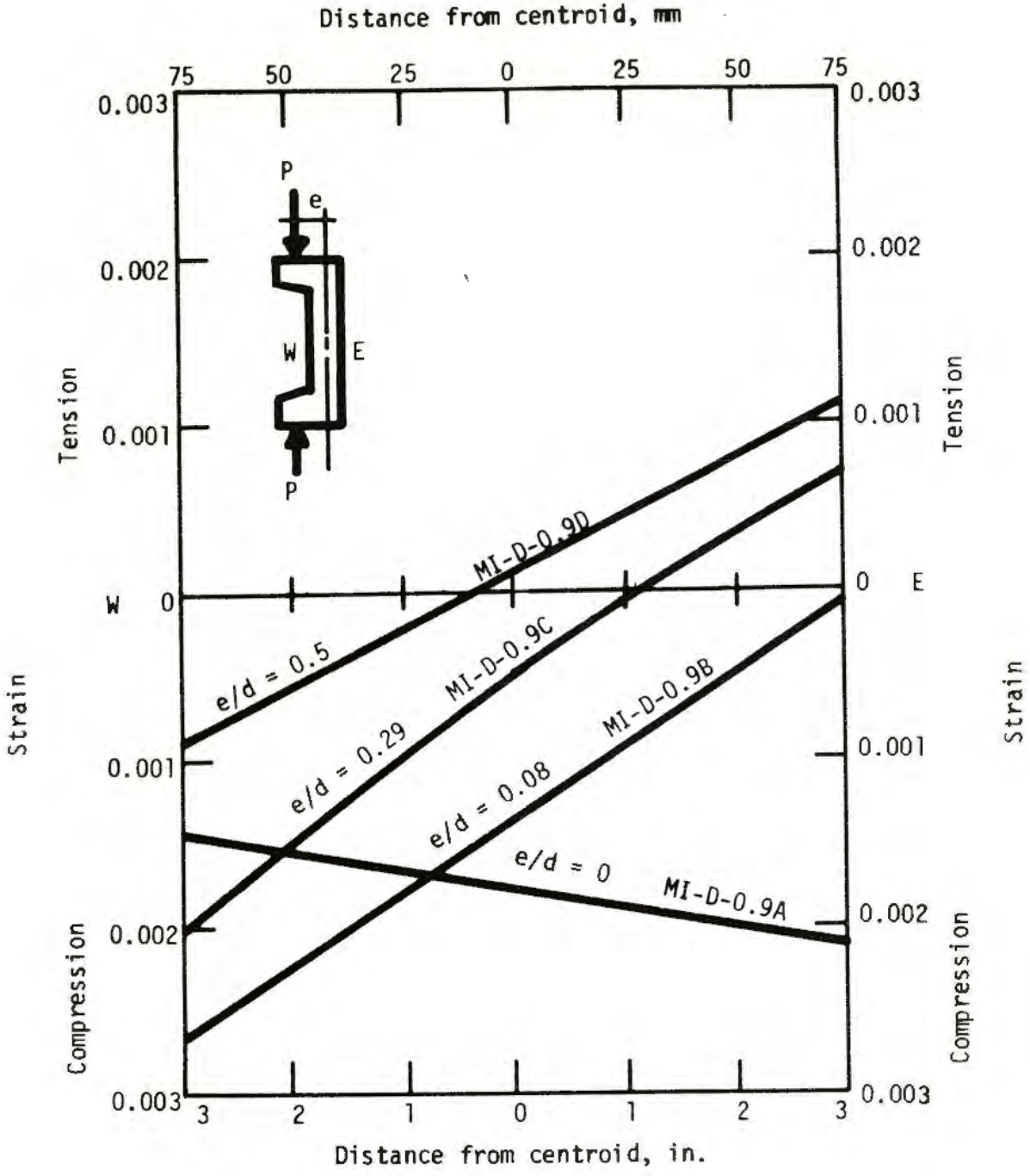

FIG. 4.7 ULTIMATE STRAIN DISTRIBUTIONS

of the concrete on the compression face. The tensile crack in this type of failure propagated almost completely through to the compression face of the specimen. Illustrations of these three types of failures are shown in Figs. 4.8, 4.9, and 4.10.

The results of specimens MI-RS-1.2C and MI-RS-1.2G are indicated separately in Fig. 4.2. All other regulated-set cement concrete beam-columns were vibrated internally at casting; while these two specimens, along with all the Duracal cement concrete specimens, were vibrated externally. It can be seen that specimens MI-RS-1.2C and MI-RS-1.2G were significantly stronger than the corresponding specimens which were vibrated internally. The fact that the compressive strength of the concrete of MI-RS-1.2C was 17 percent greater than that of MI-RS-1.2B could explain why the ultimate load of MI-RS-1.2C was 20 percent greater than that of MI-RS-1.2B, since these specimens failed primarily in compression. This same argument does not account for the fact that the ultimate load of MI-RS-1.2G was 24 percent higher than that for MI-RS-1.2F, since the compressive and flexural strengths were not significantly different for the concretes of these two specimens. The fiber distribution is more critical in a tensile failure than a compression failure. Since a tension failure entered into the failure mode of specimens MI-RS-1.2F and MI-RS-1.2G, it is reasonable to conclude that fiber distribution is affected by internal vibration, which causes a flaw that lowers the resistance of the material to tensile stresses. This study suggests that the interaction diagrams for the regulated-set underestimate the ultimate strength of the material, especially where a tension failure enters into the primary failure mode.

Values of α and β as used in ACI Code[8] in describing the distribution of compressive forces for a compression region of a flexural member at failure

FIG. 4.8 COMPRESSION FAILURE

FIG. 4.9 COMPRESSION-TENSION FAILURE

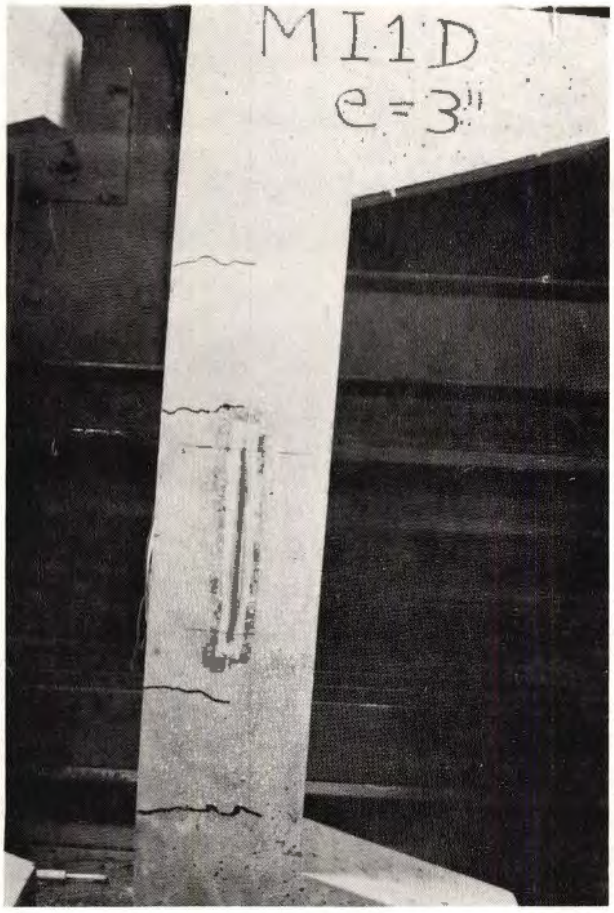

FIG. 4.10 TENSION FAILURE

are indicated in Table 4.2. These were determined from the results of specimens MI-RS-.9B, MI-RS-1.2B, MI-RS-1.2C and MI-RS-1.5B for the regulated-set cement concrete; and MI-D-.9B, MI-D-1.2B and MI-D-1.5B for the Duracal cement concrete. These specimens were chosen because the compressive strains on the tension faces of these beam columns were small at failure. Therefore, almost the entire cross section of the specimen formed a complete, fully developed compression stress block. By considering equilibrium of forces and moments on a cross section at failure, shown in Fig. 4.11, the values of α and β are determined from the following formulas:

$$\alpha = \frac{P_{max} + \frac{1}{2} E_c \varepsilon_c (c - h) b}{f_c' cb} \tag{4.1}$$

$$\beta = \frac{h}{2c} - \frac{M_{max} + \frac{1}{2} E_c \varepsilon_c (c - h)(\frac{c}{3} + \frac{h}{6}) b}{f_c' bc^2} \tag{4.2}$$

An average value of E_c taken from the cylinder tests for Poisson's ratio and Young's Modulus was used in the above equations. Since the compressive strains, ε_c, were small, the effect of any error in the value of E_c would be negligible in the above formulas. In fact, for most cases, even complete exclusion of the terms containing E_c had no influence on the calculated values of α and β.

It can be seen from Table 4.2 that the values of α and β for a given cement did not seem to be influenced by fiber content. Therefore, the results indicate that the values of $\alpha = 0.57$ and $\beta = 0.37$ may be used for regulated-set cement concrete mixes; and the values of $\alpha = 0.54$ and $\beta = 0.40$ may be used for the Duracal cement concrete mixes. The values calculated

TABLE 4.2

VALUES OF α AND β, AS DEFINED IN THE ACI CODE, FOR REGULATED-SET AND DURACAL CEMENT CONCRETES

Fiber content, percent	Cement	α	β
0.9	Regulated-set	0.55	0.36
1.2	Regulated-set	0.58	0.37
1.5	Regulated-set	0.58	0.37
0.9	Duracal	0.53	0.40
1.2	Duracal	0.56	0.40
1.5	Duracal	0.54	0.40

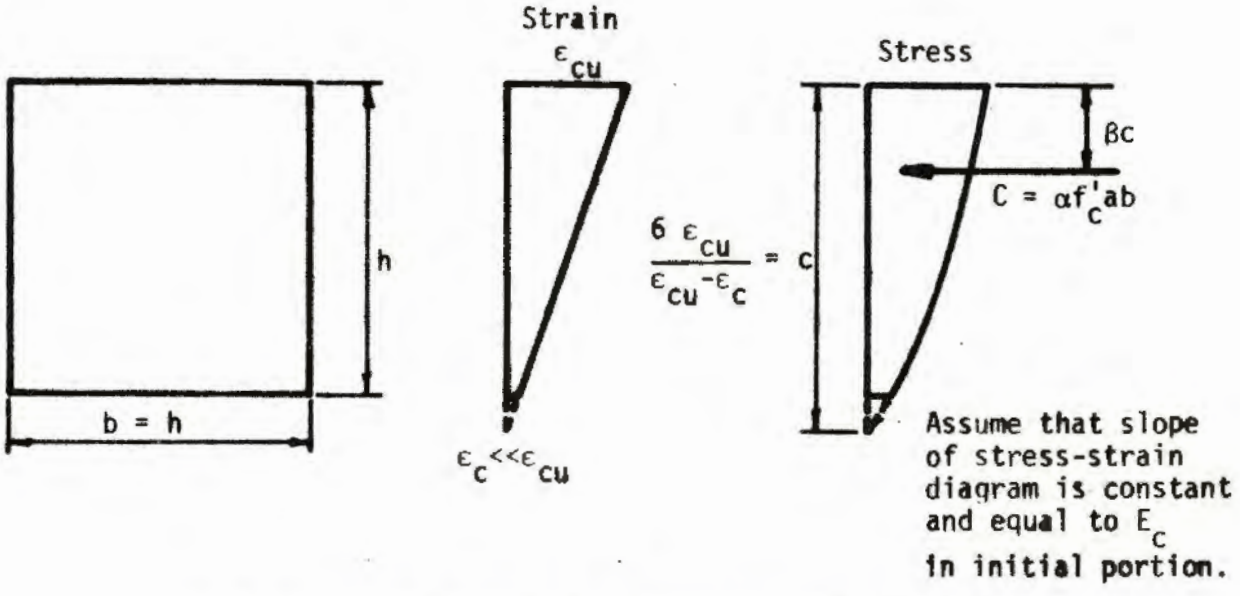

FIG.4.11 ULTIMATE STRAIN AND STRESS DISTRIBUTIONS FOR BEAM-COLUMNS

for MI-RS-1.2B and MI-RS-1.2C were both equal in spite of the difference in the method of vibration of each of these specimens. Therefore, this seems to indicate that the values of α and β for the regulated-set cement concretes were not influenced by the internal vibration.

The ultimate compressive strains measured on the compression face of the beam-column specimens when a compression failure entered into the primary failure mode are shown in Tables 1.1 and 1.2. These ultimate strains do not seem to be influenced by the fiber content of the various specimens. Therefore, in an ultimate strength analysis of a member, it may be assumed that for compression failure the strain in the outer compression fiber is about 0.0029 for the regulated set cement concretes and about 0.0023 for the Duracal cement concretes.

4.3 TENSILE STRESS-STRAIN RELATIONSHIP IN A FLEXURAL MEMBER

4.3.1 METHOD OF ANALYSIS USED TO DERIVE THE TENSILE STRESS-STRAIN RELATIONSHIP

The tensile stress-strain curves derived here indicate the average tensile stress-strain behavior of a segment of a flexural specimen surrounding a crack. This type of tensile stress-strain relationship is essential in the complete analysis of a fiber reinforced concrete in any stage of loading between first cracking and failure. The length of the segment over which the effects of cracking were distributed was assumed to be equal to the depth of the beam, with the crack located at the center of this segment, as indicated by the shaded area in Fig. 4.12a.

Only the behavior of the center portion of the beam, 36 in. (914 mm) in length and subject to a pure moment, was used to derive the tensile

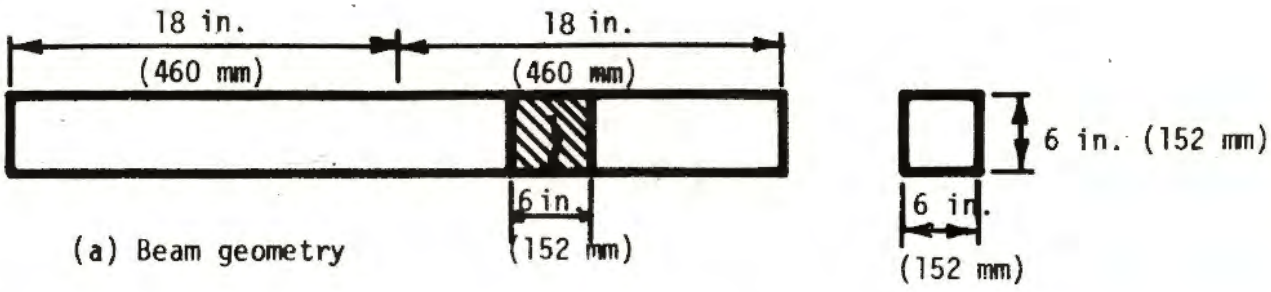

(a) Beam geometry

(b) End moments and deflected shape

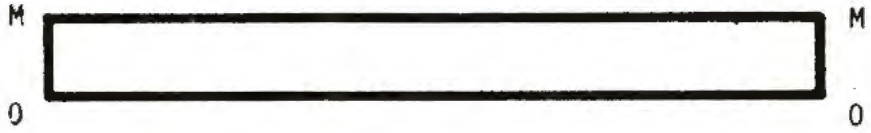

(c) Moment diagram

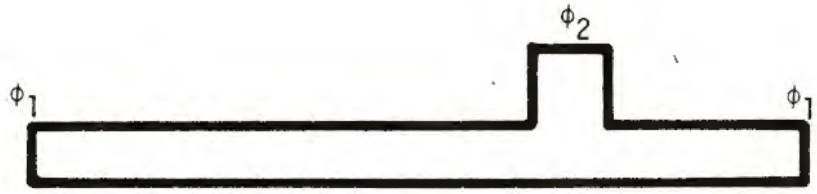

(d) Curvature diagram

FIG. 4.12 BEAM SECTION USED FOR ANALYSIS

stress-strain relation for the crack element. The center deflection of this segment was measured and plotted against load. A typical load-deflection curve for this portion of the beam is shown in Fig. 4.13a for one of the 1.2 percent fiber content flexural specimens. On this diagram, the point of slope discontinuity is the point at which cracking began in the specimen. This point of first cracking has also been noted by Snyder and Lankard.[9] The moment-curvature relation for the crack element, derived from the load-deflection curve, was used to obtain the tensile stress-strain relationship for the crack element.

In order to obtain the moment-curvature relation for the crack element from the load vs. center deflection curve for the portion of the beam subject to pure bending, the following assumptions were made:

1. The proportional limit is at the point of slope discontinuity in the load-deflection curve.
2. The curvature in the entire beam section up to the proportional limit is constant along the length and determined from $\phi = M/EI$.
3. After cracking, the material behaves linearly and elastically outside the crack element; but within the crack element, there is a uniform curvature as indicated in Fig. 4.12d by ϕ_2, which is greater than the curvature in the uncracked portion of the beam.

The moment-curvature relation in the crack element was determined under these assumptions, using the measured load-deflection curve and the moment-area theorems. A portion of the moment-curvature relation derived from the load-deflection curve in Fig. 4.13a is shown in Fig. 4.13b. The moment was determined directly from the applied load. The curvature in the crack

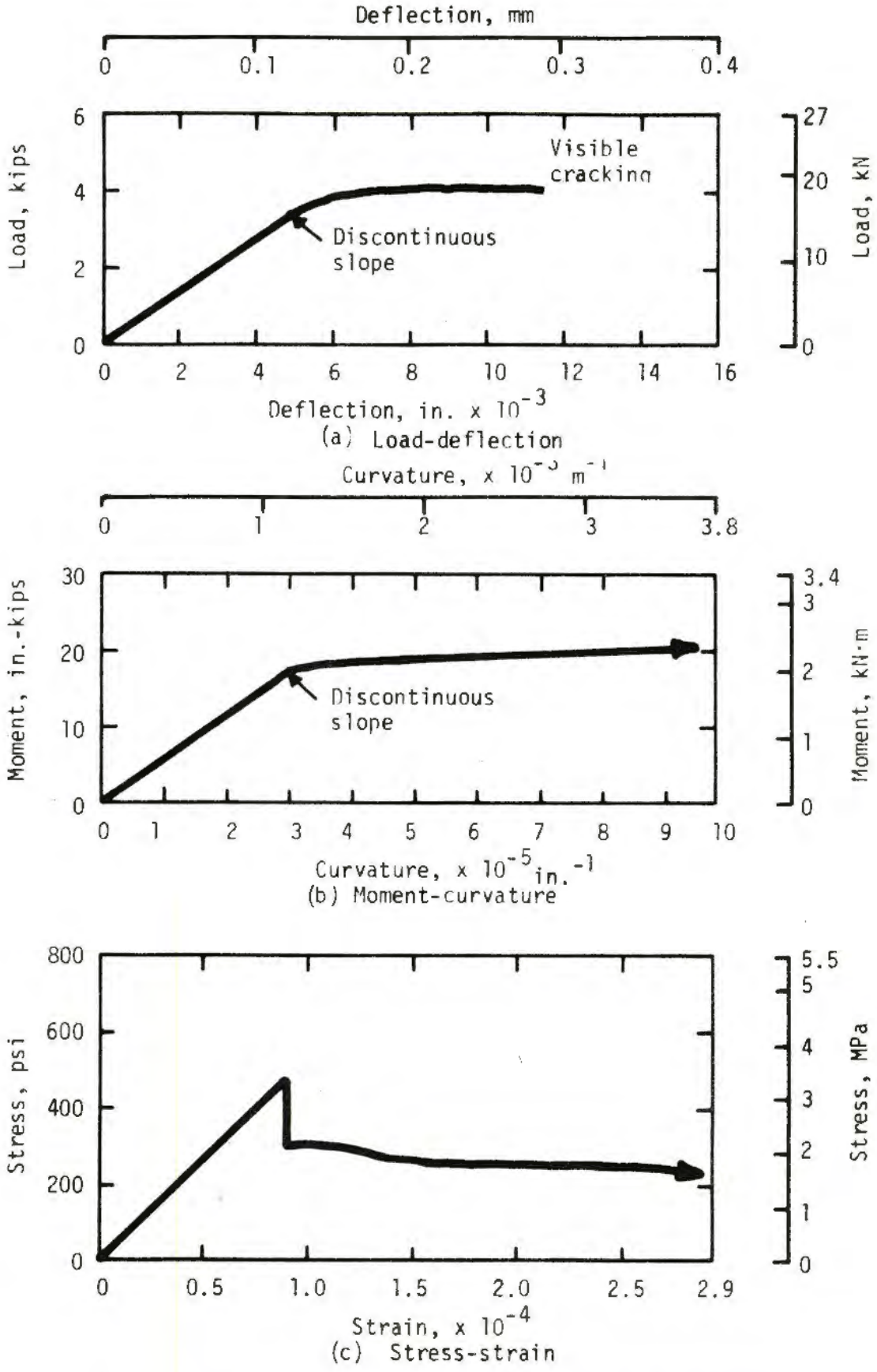

FIG. 4.13 DEVELOPMENT OF STRESS-STRAIN RELATIONSHIPS

element, ϕ_2, was the only unknown in the equations for deflections derived from the moment-area theorems.

The value of Young's Modulus, E_T, used in this analysis was determined utilizing the load, measured deflection and moment-area theorems at the proportional limit.

Once the moment-curvature for the crack element is known, the tensile stress-strain relation at cracking, and after cracking, can be found using the following reasonable assumptions:

1. The tensile stress-strain curve is linear with a slope of E_T up to the proportional limit.
2. The tensile modulus of elasticity up to cracking, E_T, is equal to the compression modulus of elasticity, E_c.
3. The compressive stress-strain relation is linear, with a slope of E_c, at all levels of loading.
4. The tensile and compressive stress-strain behavior is the same for every point within the crack element.
5. Strain variation is linear through the depth of the beam.

The arguments given below then imply that if the stress-strain curve in tension is continuous at cracking, even if a sudden change of slope is present in the stress-strain relation, the slope of the moment-curvature relationship must be continuous at cracking. However, examination of the curves of moment vs. curvature resulting from the experiments clearly shows the presence of an abrupt change of slope at cracking. It follows that the tensile stress-strain curve must exhibit a sudden drop of tensile stress at cracking.

This sharp drop in stress at the proportional limit can be explained by considering the mechanical behavior of the fiber reinforced concrete. At

the strain corresponding to tensile failure of the concrete matrix, the load carrying capacity of the material is determined only by the fibers, which are no longer acting compositely with the concrete matrix. At this point, the fibers still have the same strain and contribute the same force as just prior to the matrix cracking. Therefore, the force on a differential area must be smaller after cracking. Hence, there should be a sharp drop in stress at the cracking strain of the cement matrix.

Another substantiation of the sharp drop in stress at the proportional limit is the shape of the load-deflection curve from a uniaxial tension test of a steel-fiber reinforced concrete tensile specimen, shown in Fig. 4.14. The shape of the tensile stress-strain curve should be similar to that of a load-deflection curve obtained from a uniaxial tension test.

Under the assumption of linearly elastic behavior up to the proportional limit, the peak of the tensile stress-strain curve is defined by the equations:

$$\varepsilon_{pl} = \frac{Mh}{2E_T I} \tag{4.3}$$

$$\sigma_{pl} = E_T \varepsilon_{pl} \tag{4.4}$$

The magnitude of the stress drop was obtained by considering the slope discontinuity in the moment curvature relation, shown in Fig. 4.13b, which resulted from the slope discontinuity in the load-deflection curve.

DETERMINATION OF STRESS DROP

The stress drop at the proportional limit, $\Delta \sigma$, was determined

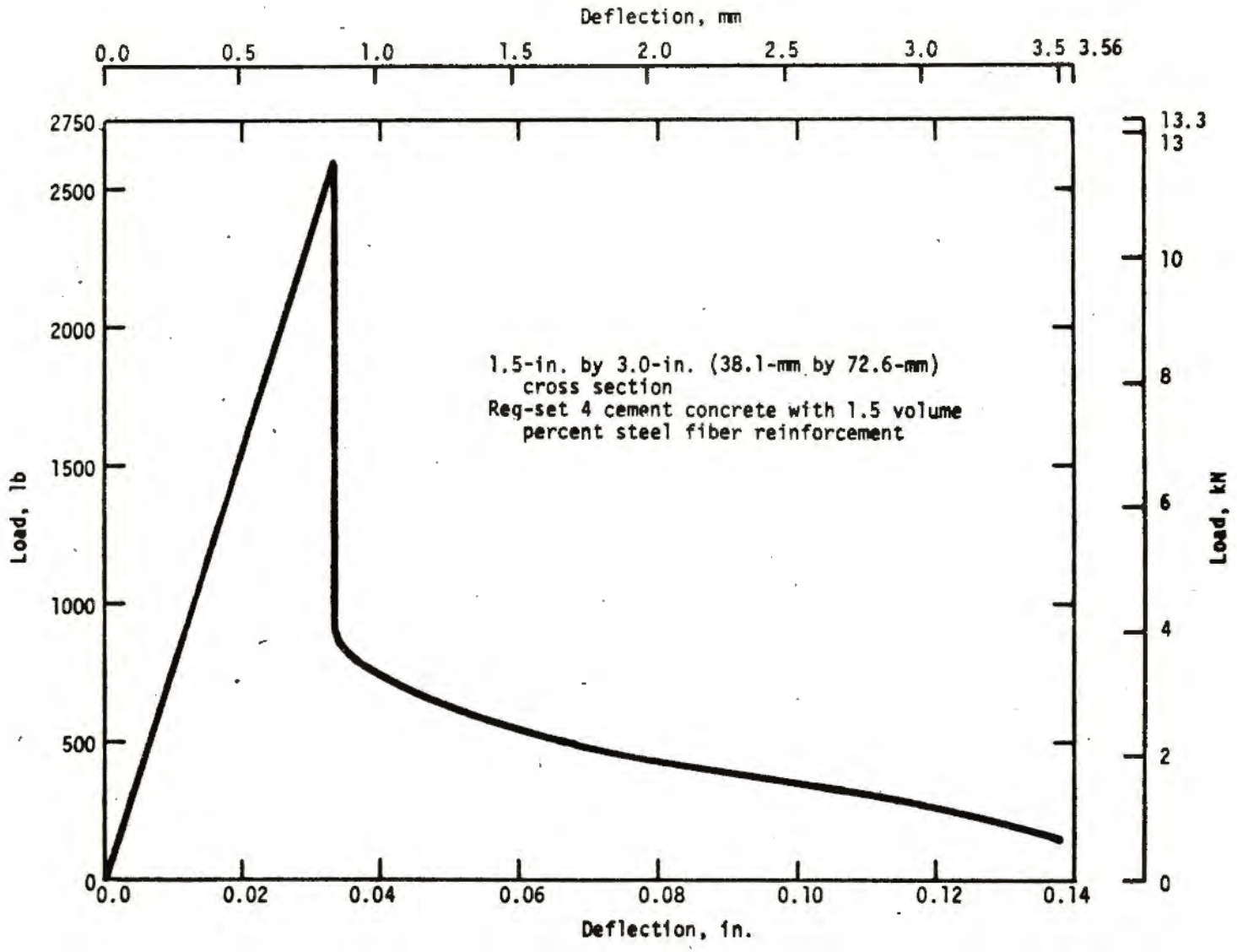

FIG. 4.14 LOAD-DEFLECTION CURVE FOR UNIAXIAL TENSION TEST

from the slope discontinuity in the moment-curvature diagram by considering equilibrium of the cross section shown in Fig. 4.15. The tensile stress, σ_x, is a function of the distance of the point from the neutral axis and the curvature, ϕ. The equilibrium equations can then be written as

$$P = \int_A \sigma_x (Z,\phi)\, dA$$

$$M = \int_A Z\, \sigma_x (Z,\phi)\, dA$$

The strain, ε_x, at any point on the cross section is given by:

$$\varepsilon_x = Z\, \phi$$

After the initiation of cracking, the compressive stresses are given by $\sigma_{x_c} = E_T Z\phi$, however, the tensile stresses are given as $\sigma_{x_t} = \sigma(Z,\phi)$. The equilibrium equations are thus:

$$P = \int_{a-h}^{0} bE_T Z\phi dZ + \int_0^a b\, \sigma_x (Z,\phi)\, dZ \qquad (4.5)$$

$$M = \int_{a-h}^{0} bE_T Z^2\phi\, dZ + \int_0^a bZ\sigma_x (Z,\phi)\, dZ \qquad (4.6)$$

Differentiation of Eq. 4.5 with respect to ϕ and the condition that P = 0 in pure bending yield the following expression, after rearrangement of terms:

$$\frac{da}{d\phi} = \frac{-\, a\, \Delta\sigma/\phi}{2\, \sigma_o + \Delta\, \sigma} \qquad (4.7)$$

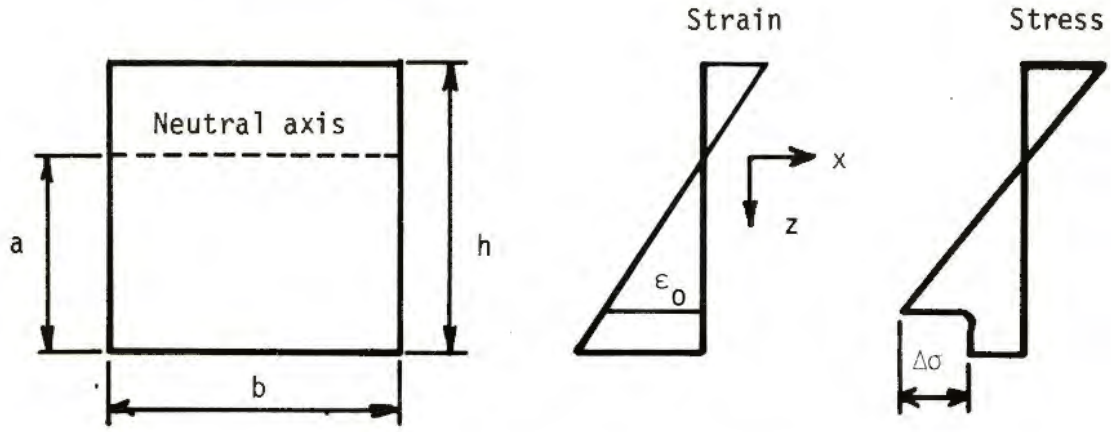

FIG. 4.15 STRAIN AND STRESS DISTRIBUTIONS FOR DETERMINATION OF STRESS DROP AT PROPORTIONAL LIMIT

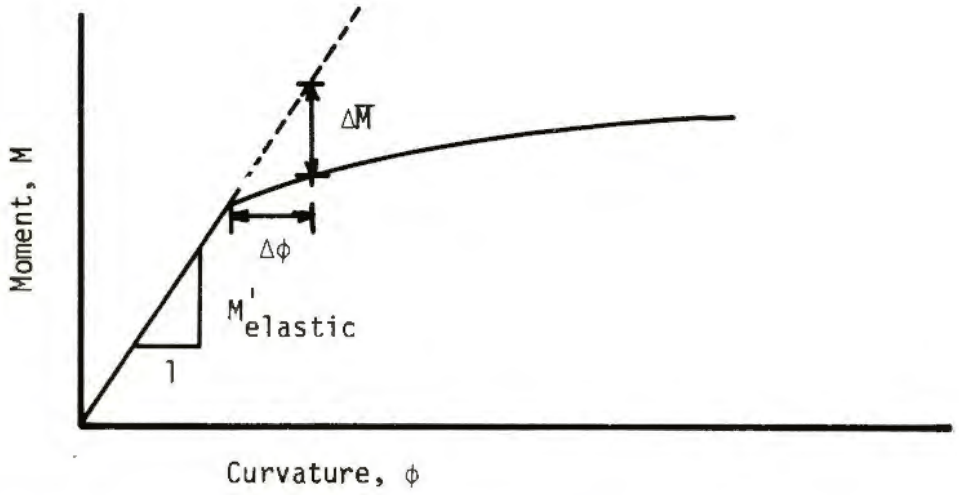

FIG. 4.16 TYPICAL MOMENT-CURVATURE DIAGRAM

where $\Delta\sigma = \sigma_x(a,\phi) - Ea\phi$ and $\sigma_o = E\phi d/2$.

In order to obtain the stress discontinuity in terms of the slope discontinuity in the M-ϕ diagram, it is necessary to express $\frac{dM}{d\phi}$ as:

$$\frac{dM}{d\phi} = \left(\frac{dM}{d\phi}\right)_{elastic} + \overline{\Delta M}' \qquad (4.8)$$

where $\left(\frac{dM}{d\phi}\right)_{elastic}$ is the initial slope of the M-ϕ curve and $\overline{\Delta M}'$ is the change in slope of the M-ϕ curve from the slope of the linear portion of the M-ϕ curve at the slope discontinuity. Differentiation of Eq. 4.4 with respect to ϕ, with the substitution of Eq.4.7 to eliminate $\frac{da}{d\phi}$ and the relation $M_{elastic} = Eb\phi d^3/12$, yields:

$$\Delta\sigma = \frac{2\,\sigma_o\,\overline{\Delta M}'}{(3\,M'_{elastic} - \overline{\Delta M}')} \qquad (4.9)$$

Equation 4.9 is the final expression used to determine the stress drop in the tensile stress-strain curve at the proportional limit.

Since the direct determination of the magnitude of a slope change in a curve presents some difficulty, it was found easiest to obtain the quantity $\overline{\Delta M}'$ in Eq. 4.9 by considering the quantities $\overline{\Delta M}$ and $\Delta\phi$ shown in Fig. 4.16. The difference between the moment found from linear extrapolation of the M-ϕ diagram beyond the slope discontinuity and the actual moment is the quantity $\overline{\Delta M}$; and $\Delta\phi$ is the curvature coordinate measured from the slope discontinuity. A relation of the form $\overline{\Delta M} = \overline{\Delta M}(\Delta\phi)$ is thus obtained. This function is then expanded in a Maclaurin's series, which results in:

$$\overline{\Delta M}(\Delta\phi) = \overline{\Delta M}(0) + \overline{\Delta M}'(0)\,\Delta\phi + \overline{\Delta M}''(0)\,\frac{\Delta\phi^2}{2} + \ldots \qquad (4.10)$$

In the above equation, $\overline{\Delta M}(0) = 0$ since the coordinate axis for the function is taken at the slope discontinuity in the M-ϕ curve.

Points near the discontinuity in the M-ϕ curve determined from experiment are considered in order to yield a plot of the log $|\overline{\Delta M}|$ vs. the log $\Delta\phi$. Near the discontinuity, this curve should be straight line, the slope of which will indicate which term of Eq. 4.10 is predominant in the portion of the M-ϕ curve near the slope discontinuity.

This procedure was followed for each of the beams tested, and it was found that the resulting log $|\overline{\Delta M}|$ vs. log $\Delta\phi$ curve was a straight line with an approximate slope of unity. This indicated that the first derivative of the function $\overline{\Delta M}$, evaluated at $\Delta\phi = 0$, was the predominant term in the series of Eq. 4.10. This can be seen by considering the equation of the line resulting from plotting log $|\Delta M|$ vs. log $\Delta\phi$:

$$\log |\overline{\Delta M}| = \log \Delta\phi + \log B \qquad (4.11)$$

where log B is the y-intercept of the log $|\overline{\Delta M}|$ vs. log $\Delta\phi$ plot. Taking the antilog of Eq. 4.11 results in:

$$\overline{\Delta M} = \Delta\phi B \qquad (4.12)$$

Comparing Eq. 4.12 to Eq. 4.10 indicates that the higher order terms of the expansion do not significantly enter into the function $\overline{\Delta M}(\Delta\phi)$ near the discontinuity. Therefore Eq. 4.10 may be rewritten in the form:

$$\overline{\Delta M}(\Delta\phi) = \overline{\Delta M}'(0)\,\Delta\phi \qquad (4.13)$$

where $\overline{\Delta M}'(0)$ is the constant, B, in Eq. 4.12 and is found by extrapolation of

the straight line of the log $|\overline{\Delta M}|$ vs. log $\Delta\phi$ plot to the point where log $\Delta\phi$ = 0. Since all of these points did not lie exactly on the straight line with a slope of unity, this extrapolation was carried out by using the best fit straight line technique for a line with a slope of unity, defined by the points calculated from the experimental log $|\overline{\Delta M}|$ vs. log $\Delta\phi$ curve. The value of $\overline{\Delta M}'$ found by using this procedure is actually a negative number. Keeping this in mind, the change of stress determined by Eq. 4.9 is actually a stress drop.

It should be pointed out here, that in order to use the above technique for the determination of $\Delta\sigma$, the line that is defined on the log $|\overline{\Delta M}|$ vs. log $\Delta\phi$ graph must have a slope of approximately unity and the best straight line through the data points, used for extrapolation, must have this slope exactly. The slightly different slope that may be calculated for the actual line using the best fit straight line technique cannot be used for extrapolation. If the actual slope of the line is significantly different from 1, the approach presented here is not valid.

DETERMINATION OF PORTION OF TENSILE STRESS-STRAIN CURVE BEYOND THE DROP IN STRESS

In order to derive the tensile stress-strain relationship beyond the drop in stress, it is necessary to use the following statical conditions:

1. The sum of compressive force and the tensile force in the beam must equal the applied axial load; and
2. The moments of the tensile and compressive forces about the center line of the cross section must be equal to the moment applied to the cross section.

As the moments and curvature increase, the compressive and tensile stresses at the outer fibers of the beam change.

Using this information and Fig. 4.17, two equations can be derived in terms of c, f_{tn}, ε_{tn}, M and ϕ, and solved to give the stress and strain at a given increment of load. The following equations were thus derived with the use of Fig. 4.17b.

From the relation P = C - T

$$P_{applied} = \frac{1}{2} E_c \phi c^2 b - \frac{1}{2} f_{t1} x_1 b - \sum_{i=3}^{n} \frac{f_{ti-1} + f_{ti}}{2} x_i b \qquad (4.14)$$

From the moment relationship

$$M_{applied} = \frac{1}{3} E_c \phi c^3 b + \frac{1}{3} f_{t1} x_1^2 b + \frac{1}{2} \sum_{i=3}^{n} [(f_{ti} - f_{ti-1}) \cdot (x_i) b \cdot ((\sum_{j=1}^{i-1} x_j) + \frac{2}{3} x_i) + 2(f_{ti-1} (x_i) b \cdot ((\sum_{j=1}^{i-1} x_j) + \frac{x_i}{2}))] \qquad (4.15)$$

In these equations, $f_{t2} = f_{t1} - \Delta\sigma$ and $x_2 = 0$. Thus, Eqs. 4.14 and 4.15, which are the basis for this method of analysis, can be written symbolically in terms of the variables:

$$P = f(c^2, f_{tn}, \phi) \qquad (4.16)$$

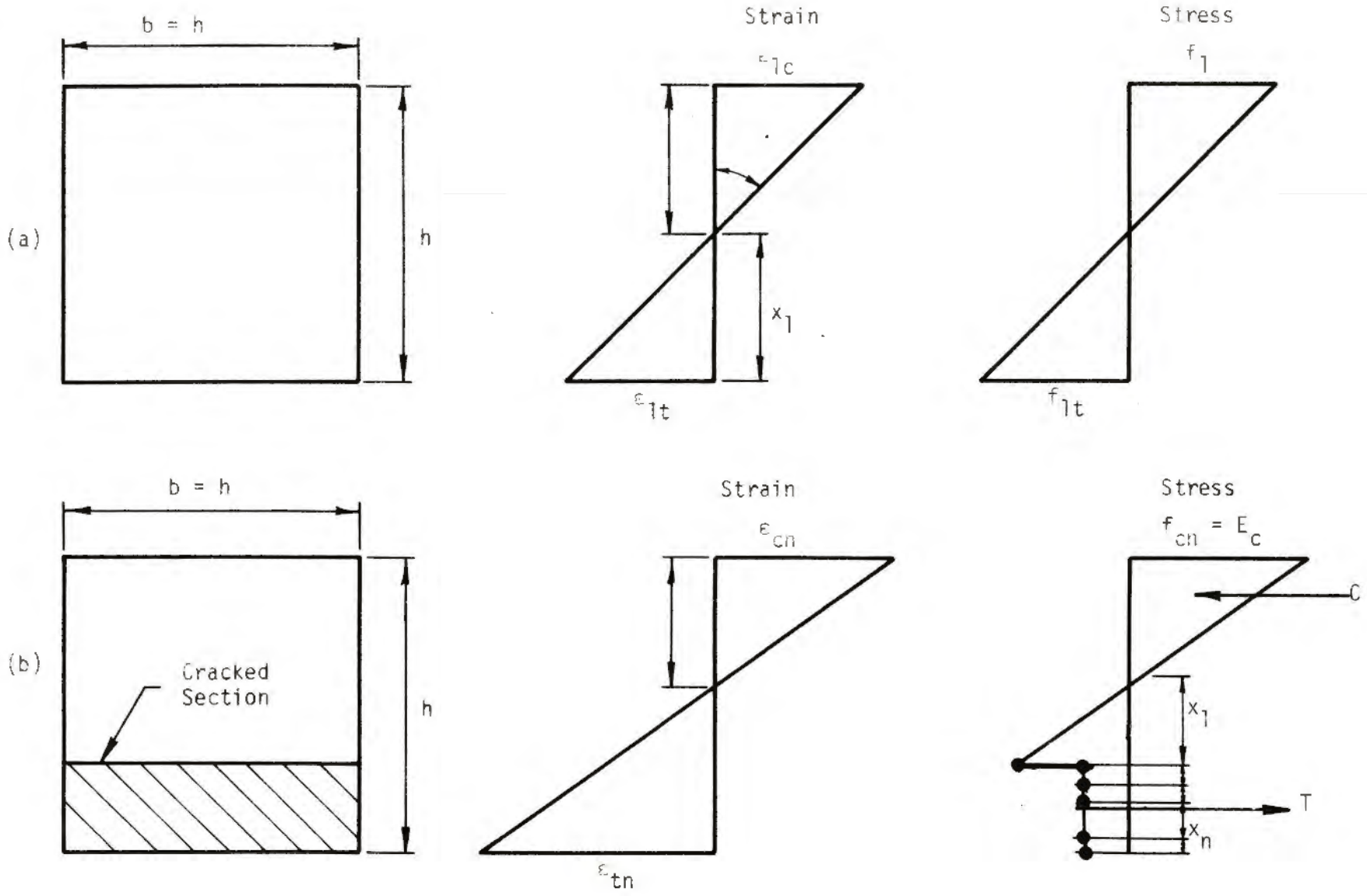

FIG. 4.17 STRAIN AND STRESS DISTRIBUTIONS IN A RECTANGULAR SECTION SUBJECTED TO PURE MOMENT

$$M = f(c^3, f_{tn}, \phi) \tag{4.17}$$

The x's are found by using strain compatibility. Once $\varepsilon_{tn} = ((h - c) \cdot \phi)$ is known, x_n can be found from the relationship

$$x_n = h - c - \sum_{i=1}^{n-1} x_i \tag{4.18}$$

The relationships were used in an iterative fashion to find the stresses and strains in tension at the outer fiber of the beam. Once a stress corresponding to a certain strain was determined, this value of stress was taken as corresponding to that strain as the curvature increased and that value of strain was reached at the interior fibers of the beam.

The iterative process employed to evaluate the real roots of the algebraic expressions given by Eqs. 4.14 and 4.15 was the Newton-Raphson method of tangents.[10] For a given increment of moment and curvature, the corresponding shift in the neutral axis and stress in the outer beam fibers necessary to satisfy equilibrium were determined by initially assuming that they had the same values as in the previous increment, and iteratively finding the new values in the present increment by calculating the change in the position of the neutral axis, $R_{n(new)} = R_{n(old)} + \Delta R_n$, and the corresponding new value of stress, $f_{tn(new)} = f_{tn(old)} + \Delta f_{tn}$, utilizing the following two equations:

$$\Delta f_{tn} = \frac{\Delta P - \left[\left(\frac{\partial P}{\partial R}\right) \frac{\Delta M}{\left(\frac{\partial M}{\partial R}\right)}\right]}{\left(\frac{\partial P}{\partial f_{tn}}\right) - \left[\left(\frac{\partial M}{\partial f_{tn}}\right) \frac{\left(\frac{\partial P}{\partial R}\right)}{\left(\frac{\partial M}{\partial R}\right)}\right]} \tag{4.19}$$

$$\Delta R = \frac{\Delta M - \Delta f_{tn} (\partial M/\partial f_{tn})}{\partial M/\partial R} \qquad (4.20)$$

where ΔP and ΔM are the difference between the applied and calculated forces and moments, respectively. Equations 4.19 and 4.20 were obtained by taking the total differential of Eqs. 4.16 and 4.17, noting that $c = \frac{h}{2} - R_n^2$, and solving the resulting simultaneous equations for Δf_{tn} and ΔR_n. At each increment, values of ΔR_n and Δf_{tn} were calculated, which yielded new values of f_{tn} and c, until equilibrium of forces and moments were satisfied by the position of the neutral axis and the stress at the outer fiber to a sufficient degree of accuracy. The next increment of moment and curvature was then taken.

The tensile stress-strain curve, computed using the above analysis technique, was subject to some oscillation. Therefore, an average, smoothed curve was drawn through the calculated points to obtain the tensile stress-strain relation for a given specimen.

The small oscillations in the tensile stress-strain curve which resulted in the analysis are inherent in this procedure for determining tensile stress-strain curve from the moment-curvature relation, since the method essentially involves a differentiation. This means that error will be magnified numerically. However, it should be kept in mind that the stress-strain relation is obtained for the primary purpose of inferring other moment-curvature relations. The oscillations in the stress-strain curves are of little importance in the subsequent computation which has the healing nature of an integration.

4.3.2 RESULTS OF ANALYSIS

The resulting "generalized tensile stress-strain curves," that is, the tensile stress-strain curves for the crack element as derived by the previous analysis, are shown in Fig. 4.18 for the Duracal cement concrete mixes with the three fiber contents of 0.9, 1.2 and 1.5 percent. These curves were obtained by taking the average of the stress-strain curves developed for the individual specimens with each fiber content. It should be noted that the curves presented here are only the average of two of the specimens with each fiber content. One of the beams with each of the fiber contents of 0.9 and 1.5 percents had slopes of the log $|\overline{\Delta M}|$ vs. log $\Delta\phi$ plot which deviated from 1 by approximately 40 and 36 percent, respectively. Therefore, results of these tests were not used for analysis, since the method for the determination of the stress drop at the proportional limit is only valid when the slope of the log $|\overline{\Delta M}|$ vs. log $\Delta\phi$ plot is approximately unity. For one of the beams with a 1.2 percent fiber content, the stress drop was about 30 percent lower than that calculated for the other beams of that fiber content. Therefore, this too was disregarded because the results did not seem to be indicative of the behavior of the material.

It will be noted in Fig. 4.18 that the strain scale only extends to 0.0007. This results from the limits that had to be placed on the deflection scale of the load-deflection curve to get the resolution necessary for the accurate determination of the slope change at the discontinuity in the moment curvature diagram, derived from the load-deflection curve.

Shown in Fig.4.13 are the total measured load-deflection curves, a

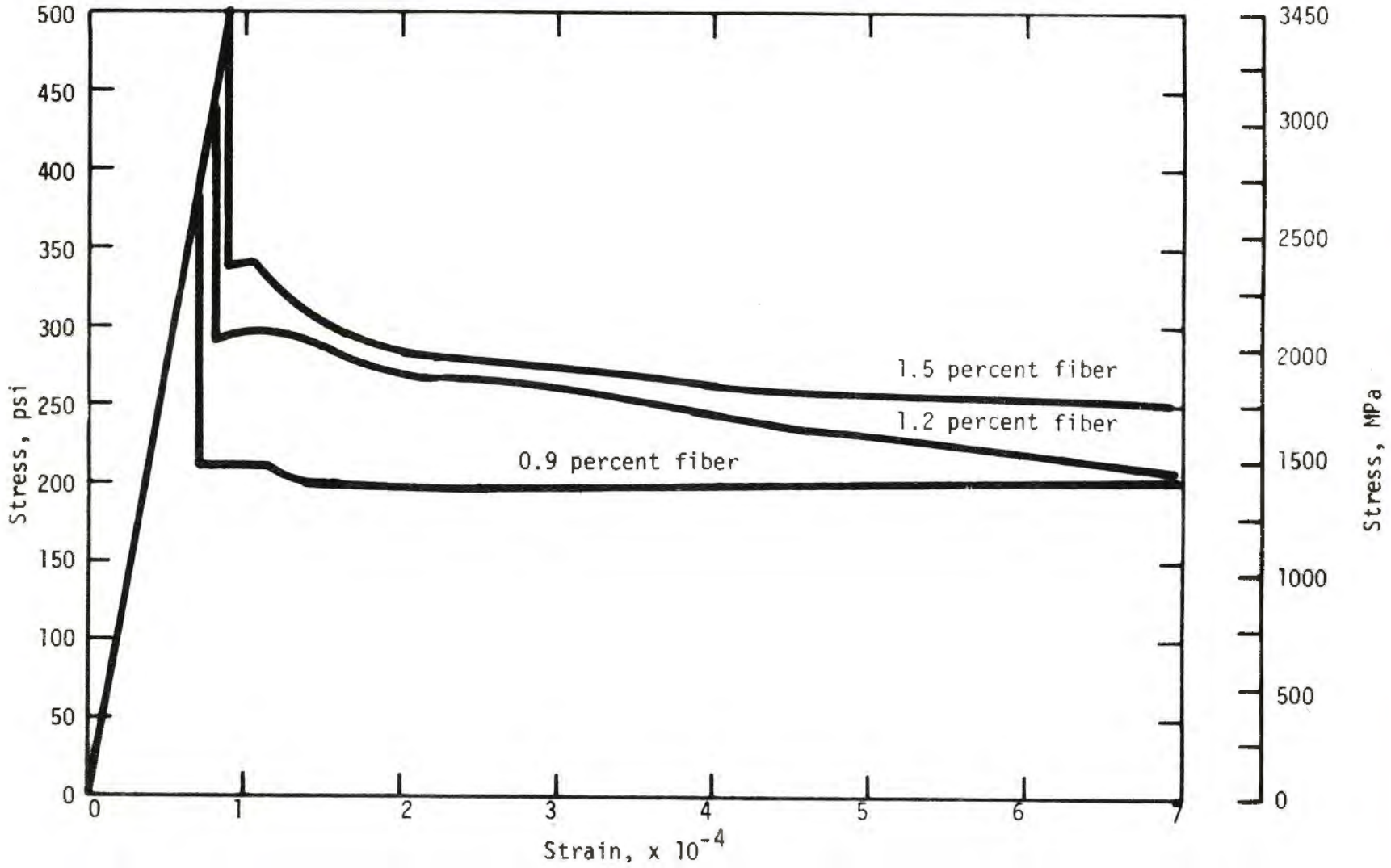

FIG. 4.18 GENERALIZED TENSILE STRESS-STRAIN RELATIONSHIPS FOR A BEAM ELEMENT--FIBER REINFORCED DURACAL CEMENT CONCRETE

portion of the resulting moment-curvature diagram, and a portion of the resulting tensile stress-strain curve for one of the specimens with a 1.2 percent fiber content. In every large flexural specimen, the maximum load was reached before the initiation of visible cracking, as indicated in Fig. 4.13a.

A comparison of the modulus of rupture computed for the 6 in. by 6-in. (150 mm by 150-mm) cross section beams and the 3 in. by 3-in. (75 mm by 75-mm) cross section beams, calculated assuming linearly elastic stress-strain behavior up to maximum load is shown in Table 4.3. Both types of specimens were cast in the same manner, yet the results indicate that the modulus of rupture is significantly lower for the larger cross section.

TABLE 4.3

EFFECT OF SPECIMEN SIZE ON APPARENT MODULUS OF RUPTURE

Fiber content, percent	f_r, psi (MPa)		Difference in apparent strength, percent	f'_c, psi (MPa)
	3 in. by 3 in. (75 mm by 75 mm)	6 in. by 6 in. (150 mm by 150 mm)		
0.9	700 (4.82)	545 (3.76)	28.3	4410 (30.4)
1.2	765 (5.27)	580 (4.01)	31.6	3950 (27.2)
1.5	840 (5.79)	680 (4.70)	23.0	4180 (28.8)

CHAPTER 5

CONCLUSIONS

5.1 DISCUSSION OF EXPERIMENTAL RESULTS

The ultimate strength interaction diagrams are presented in Figs. 4.1 through 4.6 for the regulated-set and Duracal cement concrete mixes shown in Table 2.5, with the fiber contents 0.9, 1.2 and 1.5 percent. When used in design, an appropriate factor of safety should of course be set by the designer.

As stated previously, the moment-interaction diagrams for the regulated-set cement concrete mixes may indicate lower load carrying capacity than those that would have resulted if external instead of internal vibration had been used at the time of casting. This was indicated by the significantly higher strengths of the 1.2 percent fiber content specimens which were vibrated externally when cast, and tested in the same manner as two corresponding specimens which were vibrated internally when cast. The interaction diagrams presented here for the regulated-set cement concretes are, therefore, conservative. Since internal vibration disturbs the fiber distribution at the points of vibration and causes flaws, it is not recommended that the material be vibrated internally at the time of placement. The Duracal cement concrete interaction diagrams were determined from specimens which were vibrated externally.

The results of the series of beam-columns cast using 1.2 percent fiber content regulated-set cement concrete were used to define the three types of failure and the ranges of eccentricity over which they can be

expected. At eccentricities up to approximately 0.25d, failure is caused primarily by failure of the concrete in compression with no tensile cracking; this is termed a compression failure. For eccentricities in the range of about 0.25d to 0.33d, failure of the member was caused by both crushing of the concrete on the compression face and almost simultaneous propagation of tensile cracks from the tension face to a point near the neutral axis at the interior portion of the cross section. This behavior typifies a compression-tension failure. Beyond eccentricities of 0.33d, tension failures occurred. These were characterized by failure due to the propagation of tensile cracks from the tension face to a point near the compression face, accompanied by no spalling of the concrete on the compression face.

The results given in Tables 1.1 and 1.2 for the strain at failure on the compression face for those specimens in which there was compression failure on that face indicate that in an ultimate strength design procedure the compressive strain in the outer fibers of a member for compression failure may be taken as 0.0029 and 0.0023 for the regulated-set and Duracal cement concretes, respectively. Also, from the resulting strain distributions in the beam-columns, it is reasonable to assume linearity of strain across the cross section to failure.

When using the ACI convention for defining a fully developed compressive stress block, the results indicate that the values of α and β associated with the mixes used here for the regulated-set and Duracal cement concretes with the fiber contents of 0.9, 1.2 and 1.5 percent may be taken as follows:

Regulated-set cement concrete: $\alpha = 0.57$; $\beta = 0.37$

Duracal cement concrete: $\alpha = 0.54$; $\beta = 0.40$

The generalized tensile stress-strain curves for fiber reinforced concrete are essential for a complete post-crack analysis of a structure composed of this material. This tensile stress-strain relation can be used to predict the tensile capacity of a structural member in a ultimate strength analysis. The compressive capacity is given by either the compressive stress block defined by the ACI Code when there is compression failure, or with the compressive stress block defined by the secant Young's Modulus when the compressive stress at the outer fiber at failure is up to about 50 percent of f'_c. The failure envelope is determined by the standard procedure in reinforced concrete design of assuming various strain distributions at failure and calculating the corresponding forces and moments. The tensile stress-strain curves can also be incorporated in a computer analysis of the post-crack behavior of a fiber reinforced concrete structure. It is especially important in a complete computerized analysis to have the entire tensile stress-strain relationship, rather than an equivalent tensile stress block at failure, defined by quantities similar to the quantities α and β which define the compressive stress block at failure. Those tensile stress-strain curves presented in Fig. 4.18 for the Duracal cement concrete mixes, however, are of limited use in an analysis because the experimental analysis indicated that the tensile stress can be counted upon for a considerably larger tensile strain than was foreseen when the instrumentation for the experiment was designed. Therefore, the strain scale only extends out to 0.0007.

As indicated in Table 4.3, there is a significant difference

between the modulus of rupture calculated for a 3 in. by 3-in. (75 mm by 75-mm) cross section beam and that calculated for a 6 in. by 6-in. (150 mm by 150-mm) cross section beam. Therefore, putting the interaction diagrams into a dimensionless form should not be attempted at this time.

Visible crack formation in the large flexural specimens did not occur until after they had reached their ultimate load and the load carrying capacity of the beam was decreasing. Therefore, care must be exercised when using this material at a critical section of a structure at which the ratio of moment to axial load is large, since there will be no visible indication when failure is imminent.

The modulus of elasticity and compressive strength showed a definite dependence on fiber orientation. The results given in Table 4.1 indicate that for a given mix, the modulus of elasticity will be lower if the fibers tend to be oriented perpendicular rather than parallel to the direction of stress. However, the compressive strength will be higher if the tendency of fiber orientation is perpendicular rather than parallel to the direction of stress.

The secant modulus of elasticity is presented, since this quantity gives a reasonable indication of the compressive stress-strain behavior up to approximately 50 percent of the ultimate compressive strength. The numerical values given for E_c seem to be representative of the values that can be used in design for the mixes studied here. However, representative values of E_c over a wide range of compressive strengths cannot be inferred from this study, since only two narrow ranges of compressive strengths were dealt with.

The measured values of Poisson's ratio indicate that it was influenced little by differences in cement, fiber content or direction of fiber orientation. These results indicate that a reasonable range for the value of Poisson's ratio for the mixes used in this study is 0.14 ± 0.02.

5.2 RECOMMENDATIONS FOR FUTURE RESEARCH

The tensile stress-strain curves developed here must be extended out to the point of failure. This can be readily accomplished now that there is sufficient information to determine the extent to which it is necessary to measure the load-deflection curve. The optimum length of the crack element, which was assumed to be equal to the depth of the beam in this analysis, can then be determined by assuming various values for the length of the crack element and computing the corresponding tensile stress-strain curves. These various curves can then be used to calculate theoretical values for the maximum thrust and moment that a beam-column will withstand, which can then be compared to actual beam-column test results. The most accurate theoretical prediction of ultimate loads will indicate what optimum length of crack element should be used.

In the method of analysis presented for the determination of the tensile stress-strain relation, it was assumed the the modulus of elasticity in compression was the same as that in tension because the compressive stresses which were developed in the outer fibers of the beam under pure flexure were small. This assumption should be verified.

The effect of strain rate on the behavior of fiber reinforced concrete should be studied. In the case of the tensile stress-strain curves

derived here, the stress level maintained after cracking of the concrete matrix is the result of the bond friction between the fibers and the concrete matrix as the fibers are pulling out of the concrete. If, however, there were a high enough strain rate at first cracking to cause some of the fibers to fracture, this post-crack stress level would be reduced in proportion to the number of fibers which were broken at crack initiation. Information as to the effect of strain rate on the behavior of the material would be important in the case of a fiber reinforced concrete structure subject to dynamic loading.

Since the fibers used in this study pulled out of the concrete before yielding of the steel, an attempt should be made to develop a deformed fiber with a stronger bond between the concrete and the fiber. This more efficient utilization of fiber strength would create higher post-crack strengths for a given fiber content and make it possible to achieve comparable strengths with lower fiber contents than presently used. However, care should be taken not to allow the fibers to fracture before pulling out, since the pulling out of the fibers increases the ductility, and therefore the energy absorbing capacity, of the material.

Fiber reinforced concrete containing fibers composed of a non-corrosive material, such as glass, should be investigated. If minor cracks develop at various sections in a fiber reinforced concrete structure subjected to a corrosive environment, the fibers at these sections must be able to withstand the corrosion. If the fibers did not withstand the corrosion, after a period of time there would no longer be any reinforcement.

The study of the effects of various types of fibers on the behavior of fiber reinforced concrete can be facilitated by studying the results of tests on single fibers, rather than resorting to large scale testing. This, however, requires a thorough understanding of the relationship between the results of a single fiber test and those of large scale tests. This relationship can be most easily understood by first comparing the results of single fiber tests for various lengths and angles of fiber embedment to the results of uniaxial tension and compression tests. The relationship between the uniaxial tension and compression test results and the large scale test results can then be studied. Once this progression from single fiber behavior to large scale specimen behavior is understood, it should then be possible to investigate the effect of changing the type of fiber on the behavior of a structure by studying the results of tests on single fibers.

In the beam-column specimens which failed either partially of totally in tension, it was observed that as the eccentricity decreased, so did the distance between the tension cracks which formed on the tension face of the specimens. In the beams loaded in pure flexure, only one tension crack formed. A complete analysis of a fiber reinforced concrete member, including an accurate deflection analysis, requires an indication of the number of cracks in the member, corresponding to any loading condition. Therefore, a relationship between the ratio of thrust to moment and crack spacing must be determined.

Since there was a significant variation between the moduli of rupture for the 3 in. by 3-in. (75 mm by 75-mm) cross section beams

and the 6 in. by 6-in. (150 mm by 150-mm) cross section beams, a further investigation should be conducted into the effects of changing the size and shape of a cross section on the overall behavior of a fiber reinforced concrete member. This information would be necessary to non-dimensionalize the existing experimental data on member behavior.

As previously mentioned, prediction of E_c and ν over a wide range of compressive strengths was impossible due to the two narrow ranges of compressive strengths for the mixes dealt with in this study. It is therefore necessary to determine E_c and ν for fiber reinforced concrete mixes with a wide range of compressive strengths to formulate an accurate relationship between compressive strength, and E_c and ν.

REFERENCES

1. H. F. Porter, "Preparation of Concrete from Selection of Materials to Final Disposition," V. 6, Proceedings, National Association of Cement Users, American Concrete Institute, 1910, p. 296.

2. W. Fricklen, "Improvements in Reinforced Structures and Wearing Surfaces of Hydraulic, Bituminous or Like Cement, Concrete, Asphalt or the Like," British Patent No. 11754, May 1914.

3. "Standard Specification for Deformed Billet Steel Bars for Concrete Reinforcement, A615," Book of ASTM Standards, Part 4, American Society for Testing and Materials.

4. J. Edgington and D. J. Hannant, "Steel Fibre Reinforced Concrete - The Effect on Fibre Orientation of Compaction by Vibration," V. 5, No. 25, Materiaux et Constructions, 1972, pp. 41-44.

5. "Standard Method of Test for Flexural Strength of (Using Simple Beam with Third-Point Loading, C 78," Book of ASTM Standards, Part 10, American Society of Testing and Materials.

6. "Standard Method of Test for Compressive Strength of Molded Concrete Cylinders, C 39," Book of ASTM Standards, Part 10, American Society of Testing and Materials.

7. "Standard Method of Test for Static Young's Modulus of Elasticity and Poisson's Ratio in Compression of Cylindrical Concrete Specimens, C 469," Book of ASTM Standards, Part 10, American Society of Testing and Materials.

8. "Building Code Requirements for Reinforced Concrete (ACI 318-71), American Concrete Institute, 1971, 78 pp.

9. M. J. Snyder and D. R. Lankard, "Factors Affecting the Flexural Strength of Steel Fibrous Concrete," V. 69, Proceedings, American Concrete Institute, 1972, pp. 96-100.

10. J. M. McCormick and M. G. Salvadori, "Numerical Methods in Fortran," Prentice-Hall, Inc., Englewood Cliffs, New Jersey, 1964, 324 pp.